

# Transformational process zone emerging at the tip of a propagating crack

A. Boulbitch

IEE S.A. ZAE Weiergewan, 11, rue Edmond Reuter,  
L-5326 Contern, Luxembourg;

A. L. Korzhenevskii

Institute for Problems of Mechanical Engineering,  
RAS, Bol'shoi prosp. V. O. 61,  
199178 St. Petersburg, Russia

June 30, 2019

## Abstract

Process zone at the tip of a propagating crack engendered by the stress-induced local phase transition of the second order is studied theoretically. We show that the zone can only exist within a certain domain of the phase diagram at one side of the phase transition line depending upon the sign of the striction constant. We obtain the boundary of this domain and establish its dependence upon the crack velocity. We show the existence of a critical crack velocity above which the zone cannot exist. We report the overcritical solution for the order parameter describing the incipient process zone, while far from the bifurcation point we solve the problem numerically.

## 1 Introduction

It is important to study the brittle fracture both from the point of view of numerous applications and in order to further propel our knowledge of intrinsic properties of solids. A set of experimental facts presently collected on fracture is very impressive. However, the understanding of physical aspects of the its mechanisms is still far from completeness.

Since decades a common opinion worked out that the crack behavior is determined by the process zone, a nano- to mesosized domain in the vicinity of its tip. For the long time, however, the process zone was beyond the reach of experiments. Recently new experimental techniques (described in more details below) emerged that enable one to study structure and properties of the solid in the close vicinity of the crack tip. These as well as some more traditional experimental techniques have shown that fracture is often followed by a rearrangement of the solid structure in the close vicinity of the crack tip. This challenges one to find a theoretical approach adequately describing such a phenomenon.

Stress-induced local phase transitions (LPTs) at crack tips have been reported in literature since long time. They have been observed in different classes of materials.

Stress induced austenite-martensite LPTs in metals have been studied since 60th [5] and are under a keen attention up to now. Martensite LPTs have been observed in iron [6] and steels [7], [8]. Active studies of the martensite LPT in Ni-Ti (Nitinol) alloys widely-used in

application are being actively carried out [9], [10], [11]. LPTs are also exhibited by other shape-memory alloys, such as Cu-Al-Ni [12], [13], Cr-Ni [14], Ni-Al [15] and Ti-Al-Nb [16].

Crack tip LPT from the bulk bcc phase into the nanoscale fcc phase zone has been very recently observed in molibdenum [17], the latter phase being nonexistent under pressure,  $p \geq 0$ .

ZrO<sub>2</sub> based ceramics have received a large attention, since it has been observed that the tetragonal-monoclinic phase transition at the crack tip strongly improves their fracture toughness [19], [20] [21]. Ferro- and antiferroelectric ceramics have also been reported to exhibit LPT under fracture [22], [4].

The fracture toughness improvement due to the superconducting LPT in YBCO and BSCCO at the crack tip has been reported in the paper [23].

A structural rearrangement within the crack tip zone in sapphire manifested in formation of metastable Al-O-Al clusters at its fracture surface has been recently reported [24].

The crack tip stress-induced structural LPTs have been also observed in polymers and epoxies [25]. Resins are known to exhibit crystallization at the crack tip strongly affecting the fracture process [26].

As for general trends in the evolution of the methods of the LPT observation one can note a transition from indirect methods of analysis to those making it possible to obtain a direct structure of the transformed zone with a high spatial resolution, combining few techniques in one study often appropriate for propagating cracks. One should first of all mention the method of high-angle annular dark-field scanning TEM approach allowing for the direct imaging of atomic locations. It is this method that has been recently used to detect the crack tip LPT in molibdenum. To exclude any interpretation ambiguity the results have been further combined with the electron nanodiffraction patterns [17]. Further, the combination of micromechanical loading with *in-situ* high-resolution X-ray microdiffraction [10] enabled the authors to image a complex LPT zone in the polycrystalline Nitinol. The combination of the *in-situ* SEM with the electron backscatter diffraction [8] made it possible to study the evolution of the emerging phase in the tip vicinity during the fatigue experiments. The *in-situ* optical digital image correlation technique made it possible to obtain strain fields and the phase boundaries at the tips of propagating cracks [11]. Raman mapping revealed the local distribution of phases in the vicinity of the crack tip [4]. AFM maps the lateral distribution of the surface height. The latter is directly related to spontaneous phase transition strain, thus, enabling one to distinguish phases and determine the phase boundary [3], [13].

On the theoretical side three approaches can be pointed out. First, atomistic mechanisms of LPTs have been revealed by computer simulations and density functional theory-like calculations for several solids, such as iron [27], [28], [29], silicon [30], [31], [32], tantalum [33], zirconium [34], UO<sub>2</sub> [35], molibdenum [17], Nitinol [36]. This became possible as the result of the computation power development, and advancement of the molecular dynamics approach, as well as in implementation of hybrid approaches combining the molecular dynamics with quantum mechanics [32]. The simulations revealed a strong dependence of the LPT formation upon (i) loading mode, (ii) crack plane and direction and (iii) sample geometry [27], [28]. They further elucidated atomistic mechanisms leading to the LPT development [28], [32].

Second, a number of researches exploited a mechanical approach treating the LPT zone as the one only differing from the rest of the solid by its (i) elastic properties and (ii) spontaneous strain. Antolovich [18] was first to propose a mechanism of the transformation toughness of a quasi-static crack. References to further papers of this kind one finds in the reviews [19], [20] [21] as well as in the book [46].

The above approach ignores the fact that the local phase transition is related to one or several internal degrees of freedom of the solid obeying their intrinsic constitutive laws. A third stream of works just focused on the role of the internal degrees of freedom in the

formation of the LPT at extended defects. It has been pioneered by the paper of Nabutovsky and Shapiro describing the dislocation-induced LPT [47]. In the papers of Korzhenevskii the effect of the LPT on the behavior of dislocations and, thus, on plastic properties of the solid has been established [48], formation of the LPT at a moving dislocation has been described in the paper [49]. LPT at wide domain walls has been described in [50], while those at narrow twin boundaries has been addressed in the papers [51]. This approach has also been developed in application to brittle fracture. Formation of the LPT at the crack tip has been analytically described in the papers [52] and [53], and numerically in [54] and [55].

It is generally accepted that mechanisms of the brittle solid resistance to the crack propagation are attributed to its process zone (PZ). The PZ notion only has sense, if such a zone can be clearly distinguished from the bulk of the solid. The latter can only be done, if at least one its physical property exhibits a perceptible variation across the PZ boundary. It may either be an abrupt quantitative variation such as the elastic nonlinearity [43] or hyperelasticity [42], or any qualitative variation. In the latter case the PZ differs from the bulk by e.g. its chemical composition or crystal structure. Such properties determining qualitative differences are always controlled by internal solid degrees of freedom,  $\eta$ , as e.g., concentration of reaction species in the former and phonons, magnons, electronic degrees of freedom, etc. in the latter case.

We focus on the case of the PZ qualitatively different from the solid bulk by its structure described. Condensation of any such structural degree of freedom in the bulk of the solid ( $\eta = \text{const} \neq 0$ ) corresponds to a bulk phase transition (PT): structural, magnetic, electronic respectively. The degree of freedom related to the condensate,  $\eta$ , is referred to as the "order parameter".

High values of stress at the crack tip:  $\sigma \sim r^{-1/2}$  may trigger formation of a transformational PZ, where  $\eta = \eta(\mathbf{r}) \neq 0$  within the zone, while vanishing outside. This situation may, thus, be regarded as a LPT. Here  $\sigma$  is the stress tensor and  $\mathbf{r}$  is the radius-vector counted off from the crack tip [39].

The present paper reports the case of the second order LPT admitting a fully analytical treatment. The latter is of a paramount importance, since it gives hints of what can be expected in more complex cases that cannot be treated analytically.

We show here that in a solid undergoing a second order phase transition a LPT zone with the size

$$L_f \sim 10 \left( \frac{g}{a|k|K_I} \right)^{2/3} \quad (1)$$

forms at the tip of the motionless as well as propagating crack either above, or below the line of the phase transition on the phase diagram. We show that in the both cases the difference,  $T_* - T_c$ , between the transformational process zone (TPZ) emerging temperature,  $T_*$ , and the bulk transition temperature (the Curie point),  $T_c$ , is

$$T_* - T_c \sim \pm \left( \frac{a}{g} \right)^{1/3} (|k|K_I)^{4/3} \mp \frac{\kappa^2 V^2}{4ga} \quad (2)$$

The difference,  $\Delta T_* = T_* - T_c$ , we refer to as the "temperature shift". Here  $K_I$  is the stress intensity factor applied to the crack,  $E$  is the Young's modulus,  $k = dT_c/dp$  is the slope of the phase transition line in the  $(p, T)$  phase diagram,  $\kappa$  is the order parameter kinetic constant and  $g$  is the one defining the energy of the order parameter inhomogeneity, the parameter  $a$  is related to the Curie constant,  $C$  as  $a = 2\pi/C$ . The upper sign corresponds to  $k < 0$ , while the lower one - to  $k > 0$ . Therefore, if the phase diagram slope is positive ( $k > 0$ ), the LPT only takes place below the phase transition line in the phase diagram  $\Delta T_* < 0$ , while the negative slope ( $k < 0$ ) results in  $\Delta T > 0$ , that is, the zone containing a low-temperature phase is embedded into the matrix of a high-temperature phase (1).

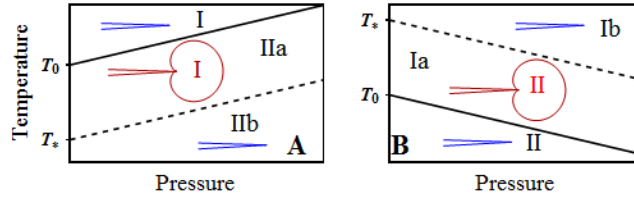


Figure 1: Schematic view of the location of the process zone on the phase diagram depending upon the slopes of the transition lines. (A) The bulk phases I and II are separated by the phase transition line,  $T_0(p)$  (the solid line), with  $k > 0$ . The region of the process zone existence, IIa, is below the transition line, where the phase I process zone is embedded into the matrix of the bulk phase II. In the region IIb, below the line  $T_*(p)$  (the dashed line) the process zone vanishes. (B) The case of the negative slope,  $k < 0$ , of the bulk phase transition line,  $T_0(p)$  (solid). The process zone existence region, Ia, is situated above the phase transition line, where the phase II is embedded into the matrix of the phase I. In the region Ib above the  $T_*(p)$  line (dashed) the zone vanishes.

We, further, demonstrate the existence of the critical velocity:

$$V_c \sim \frac{g^{1/3}}{\kappa} (a |k| K_I)^{2/3} \quad (3)$$

such as soon as the crack tip velocity exceeds the critical one, the TPZ vanishes.

In the discussion we first illustrate the results using the examples of few ferroelectrics: BaTiO<sub>3</sub>, PbTiO<sub>3</sub> and LiNbO<sub>3</sub>. We, further, estimate typical values of  $\Delta T_*$ , valid for most inorganic solids. This represents our most striking result. Indeed, the typically  $\Delta T_*$  values lie between  $\sim 10^2$  and  $\sim 10^3$  K. This implies that the TPZ existence region covers a considerable part, if not the whole phase diagram, though only at one side of the phase transition line. We then discuss experimental difficulties of the TPZ detecting, as well as possible ways of its observation. We, finally, put forward a general approach for the concept of the process zone.

The paper is organized as follows. In Section II we formulate an equation describing the order parameter dynamics. Lengthily details of its derivation we give in Appendix A. In Section III we find the analytical solution of the PZ equations. In Section VI we report our numerical results. In Section V we make numerical estimates and give comments generalizing our findings.

## 2 Process zone dynamics

Dynamic behavior of the order parameter splits into several universality classes as it is suggested by the Hohenberg-Halperin-Ma scheme [57]. Within this scheme the most simple and simultaneously most often met case is referred to as the model A describing the dynamics of a nonconserved order parameter,  $\eta$ , corresponding to a phase transition.

We focus on the case related to crystal structure variation within the process zone, that is, the case of a structural LPT. For PTs of such a type the order parameter generally represents a multicomponent object,  $\eta = (\eta_1, \eta_2, \dots, \eta_n)$ , each component being composed of combinations of displacements of the unit crystal cell atoms. Its properties are completely determined by the corresponding irreducible representation of the crystal symmetry group in the high-symmetry phase of the solid [58], [59], [60]. In the high-symmetry phase  $\eta = 0$ , while in the bulk low-symmetry phases the components  $\eta_i$  ( $i = 1, 2, \dots$ ) of the order parameter, are

either equal to constants, or to zero. They are independent of spatial coordinates, at least within a single domain of a given phase. Such an approach introduced by Landau in 1937 [58] enables one to classify all phases and to predict possible bulk phase diagrams [59], [60]. Here we adapt this approach for the description of the local transformational PZ.

In this paper we only consider the case of a single-component order parameter ( $n = 1$ ). Being simple it already catches the most important properties of the dynamic LPTs. It is also important for another reason. One observes that in solids with PTs described by multicomponent order parameters, most of their bulk low-symmetry phases are described effectively by one independent parameter. For example, the low-symmetry phases in BaTiO<sub>3</sub> are generally described by the three-component polarization vector  $\eta = (\eta_1, \eta_2, \eta_3)$ . However, in the tetragonal phase one finds  $\eta = (0, 0, \eta)$ , in the rhombohedral phase -  $\eta = (\eta, \eta, \eta)$  and in the orthorhombic phase -  $\eta = (\eta, \eta, 0)$ : all these phases are, thus, effectively single-component ones. This situation is characteristic also for structural PTs in many other materials. This makes the case of the single-component order parameter distinguished.

## 2.1 Equation of motion for the order parameter

Equation describing the order parameter dynamics can be obtained with the help of the dissipation function:

$$D = \frac{\kappa}{2} \int \left( \frac{\partial \eta}{\partial t} \right)^2 d\Omega \quad (4)$$

and the free energy:

$$F = \int \Phi(\eta, \varepsilon_{ik}) d\Omega \quad (5)$$

where  $\kappa$  is the kinetic constant,  $t$  is the time,  $\Phi = \Phi(\eta, \varepsilon_{ik})$  is the free energy density,  $\varepsilon_{ik}$  is the strain tensor and  $\Omega$  is the domain. Since we consider a thin plate case here,  $\Omega$  represents a plane and  $d\Omega \equiv dxdy$ . That is, we assign both  $F$  and  $D$  to the unit solid thickness in the  $z$  direction.

Here we address the simplest case of a PT describing by a one-component order parameter. In the one-component case the only possible transformations under the action of the crystal symmetry group are either  $\eta \rightarrow \eta$  or  $\eta \rightarrow -\eta$ . Being invariant with respect to the crystal symmetry, the free energy should only contain even functions with respect to  $\eta$  [58]. It takes the following form:

$$\Phi(\eta, \varepsilon_{ik}) = \Phi_{\text{pt}}(\eta) + \Phi_{\text{el}}(\varepsilon_{ik}) + A\eta^2\varepsilon_{ii} \quad (6)$$

Here  $\Phi(\eta, \varepsilon_{ik})$  is the free energy density, the function  $\Phi_{\text{pt}}(\eta)$  denoting its part responsible for the PT itself:

$$\Phi_{\text{pt}} = \frac{g}{2} (\nabla \eta)^2 + \frac{\alpha}{2} \eta^2 + \frac{\beta_0}{4} \eta^4 \quad (7)$$

where  $g > 0$ , and  $\beta_0 > 0$  are the constant parameters of the Landau potential (5), while  $\alpha = a(T - T_c)$ , where  $a > 0$  is a constant,  $T$  is the temperature and  $T_c$  is the Curie temperature and  $\nabla \eta$  is the order parameter gradient. The case of the first order transition  $\beta_0 < 0$  will be analyzed elsewhere. The strain tensor,  $\varepsilon_{ik}$ , is defined in a usual way:

$$\varepsilon_{ik} = \frac{1}{2} \left( \frac{\partial u_i}{\partial x_k} + \frac{\partial u_k}{\partial x_i} \right)$$

Here  $u_i$  is the displacement vector.

$\Phi_{\text{el}}(\varepsilon_{ik})$  is the elastic part of the free energy density. For simplicity we consider here the elastically-isotropic case with

$$\Phi_{\text{el}} = \frac{\lambda}{2}\varepsilon_{ii}^2 + \mu\varepsilon_{ik}^2 \quad (8)$$

where  $\lambda$  and  $\mu$  are Lamé constants [66], where

$$\lambda = \frac{E\nu}{(1-2\sigma)(1+\sigma)}; \quad \mu = \frac{E}{2(1+\sigma)} \quad (9)$$

yields their relations to the Young's modulus and Poisson's ratio,  $\sigma$ . The latter should not be confused with the stress tensor  $\sigma \equiv \sigma_{ik}$ . It should be mentioned that the constants  $g$ ,  $a$ ,  $\beta$ ,  $T_c$  and  $A$  represent the material constants of the solid in question together with  $E$  and  $\sigma$ .

Finally, the, so-called, striction constant,  $A$ , already introduced above is responsible for the interaction between the strain and order parameter fields and can be either positive or negative. It should be noted that the form of the interaction term  $A\eta^2\varepsilon_{ii}$  in (6) implies that the phase transition only gives rise to the spontaneous dilatation. It is only this case that is considered in the present paper. Our final results are more convenient to express in terms of the slope of the phase transition line,  $k = dT_c/dp$ , on the  $(p, T)$  phase diagram directly related to the striction constant  $A$ . Indeed, one can represent the term  $\sim \eta^2$  in (6, 7) as  $a(T - T_c + Aa^{-1}\varepsilon_{ii})\eta^2$ , yielding

$$k = \frac{A(1-2\sigma)}{aE} \quad (10)$$

Equation of motion can be built on the basis of (5, 4) as follows [58]:

$$\frac{\delta D}{\delta \eta} = -\frac{\delta F}{\delta \eta}; \quad \frac{\delta F}{\delta \varepsilon_{ik}} = 0 \quad (11)$$

where  $\delta$  is the variation sign. One obtains the following system of equations:

$$\begin{cases} \kappa \frac{\partial \eta}{\partial t} = g\Delta\eta - [\alpha - 2A\varepsilon_{ii}(\mathbf{r})]\eta - \beta_0\eta^3 \\ \partial\sigma_{ik}/\partial x_k = 0 \end{cases} \quad (12)$$

where  $\Delta$  is the Laplace operator and  $\sigma_{ik} = \partial\Phi/\partial\varepsilon_{ik}$  is the stress tensor:

$$\sigma_{ik} = \lambda\varepsilon_{jj}\delta_{ik} + 2\mu\varepsilon_{ik} - A\eta^2\delta_{ik} \quad (13)$$

Here  $\delta_{ik}$  is the Kronecker symbol. The last term,  $A\eta^2\delta_{ik}$ , in the expression (13) describes the spontaneous stress generated by the phase transition. For simplicity we omitted the inertial term in the second Eq. (12), which is valid, if  $V \ll c$ , where  $c$  is the sound speed.

Equations (12, 13) represent the complete system describing the dynamics of the transformational PZ.

One can eliminate the elastic degrees of freedom,  $\varepsilon_{ij}$ , from the equations of motion (12) as it is described in details in Appendix A. After their elimination one comes to the single equation of motion or the order parameter:

$$\kappa \frac{\partial \eta}{\partial t} = g\Delta\eta - [\alpha + 2A\varepsilon_{ii}^{(0)}(\mathbf{r})]\eta - \beta\eta^3 \quad (14)$$

In contrast to the strain tensor  $\varepsilon_{ii}(\mathbf{r})$  met in Eq. (12) describing both the field of the tip and that generated the PZ, the tensor  $\varepsilon_{ik}^{(0)}(\mathbf{r})$  only describes the strain field of the "undressed" tip, i.e., the one without the LPT ( $\eta \equiv 0$ ). It is given by the well-known fracture theory expression [39]:

$$\varepsilon_{ii}^{(0)}(\mathbf{r}) = \frac{(1+\sigma)(1-2\sigma)K_I}{E(2\pi r)^{1/2}} \cos(\theta/2) \quad (15)$$

where  $r$  and  $\varphi$  are the polar coordinates counted off from the crack tip and  $\sigma$  is the Poisson's ratio. The parameter  $\beta$  is expressed in terms of  $\beta_0$  (7, 12) as follows:

$$\beta = \beta_0 \left\{ 1 - \frac{2A^2}{E\beta_0} \frac{(1-2\sigma)(1+\sigma)}{1-\sigma} \right\} \quad (16)$$

Equation (14) exhaustively describes the order parameter dynamics within the PZ. It should be mentioned that (14) can be obtained by the variation procedure (11) using the dissipation function (4) and the effective free energy:

$$F_{\text{eff}} = F_0 + \int \left[ \frac{g}{2} (\nabla \eta)^2 + \frac{1}{2} \alpha \eta^2 + \frac{1}{4} \beta \eta^4 + A \eta^2 \varepsilon_{ii}^{(0)}(\mathbf{r}) \right] d\Omega \quad (17)$$

derived in the Appendix A.

For the sake of completeness let us also mention that in the equilibrium ( $\partial \eta / \partial t = 0$ ), homogeneous ( $\Delta \eta = 0$ ) state, away from the tip ( $\varepsilon_{ii}^{(0)} = 0$ ) one finds the bulk phase  $\eta = 0$  also referred to as the "mother phase" at  $T > T_c$ , while at  $T < T_c$  the bulk "daughter phase",  $\eta = \pm (-\alpha/\beta)^{1/2}$  takes place [58].

Equation (14) represents the model A according to the Hohenberg-Halperin-Ma scheme [57]. Its solution is demonstrated in Section III.

### 3 Analytical analysis of the equation of motion for the order parameter

#### 3.1 The automodel regime

Assuming the crack tip propagating with the velocity  $V$  along the  $Ox$  axis and passing to the comoving frame,  $x' = x - Vt$ ,  $y' = y$ , one finds the equation of motion (14) in the form:

$$g \Delta \eta + \kappa V \frac{\partial \eta}{\partial x'} - \left[ \alpha \pm B \frac{\cos(\theta)}{\sqrt{r'}} \right] \eta - \beta \eta^3 = 0 \quad (18)$$

where

$$B = 2 \sqrt{\frac{2}{\pi}} a |k| (1 + \sigma) K_I > 0 \quad (19)$$

and one chooses the sign "+", if  $A > 0$  and "-" in the opposite case. Further,  $r' = (x'^2 + y'^2)^{1/2}$ , and the Laplace operator is defined as  $\Delta = \partial^2 / x'^2 + \partial^2 / y'^2$ . From here on we only use the comoving frame and, therefore, omit the primes.

If one describes a transformational PZ  $\eta(\mathbf{r}) \neq 0$  embedded into the matrix of the bulk phase ( $\alpha > 0$ ,  $\eta = 0$ ), localized at the crack tip,  $(x, y) = 0$ , while vanishing away from it, the boundary condition takes the form:

$$\eta(\infty) = 0 \quad (20)$$

Because its physical origin is related to atomic coordinates which must be limited, the order parameter is everywhere finite:  $|\eta| < \infty$  [61].

For the description of the order parameter distribution embedded into the matrix of the daughter phase: ( $\alpha < 0$ ;  $\eta = (-\alpha/\beta)^{1/2} \neq 0$ ), one needs to use the boundary condition:

$$\eta(\infty) = (-\alpha/\beta)^{1/2} \quad (21)$$

Below to study the problem at hand we employ methods of the bifurcation theory.

## 3.2 Bifurcation theory: a brief review

For the convenience of the reader let us first shortly recite some key results of theory of bifurcations [68] which we use in the following argumentation. Let us consider a nonlinear equation that can be written in the form:

$$\hat{L}(\alpha)\eta = \hat{N}(\eta) \quad (22)$$

where  $\hat{L}(\alpha)$  is a linear operator depending upon the parameter  $\alpha$ ,  $\eta = \eta(\mathbf{r})$  is a dependent function and  $\hat{N}(\eta)$  is a nonlinear operator, such that  $\hat{N}(0) = 0$ . In general both  $\hat{L}(\alpha)$  and  $\hat{N}$  can be differential, integral or integro-differential operators. In the case considered in our further study  $\hat{L}(\alpha)$  is a differential operator, while  $\hat{N}$  is a polynomial.

One can see that equation (22) has a trivial solution  $\eta = 0$ . Assume that it is stable at some  $\alpha > 0$ . The trivial solution of (22) becomes unstable, as soon as  $\alpha$  reaches  $\alpha_* > 0$ , equal to the first eigenvalue,  $\alpha_* = \alpha_1$ , of the linearized equation (22):

$$\hat{L}(\alpha_n)\Psi_n(\mathbf{r}) = 0 \quad (23)$$

Here  $\alpha_n$  are the eigenvalues belonging to the discrete spectrum of the equation (23), if any,  $\Psi_n(\mathbf{r})$  are their corresponding eigenfunctions and  $n = 1, 2, \dots$  are the natural numbers. In analogy with quantum mechanics  $\alpha_* \equiv \alpha_1$  and  $\Psi_*(\mathbf{r}) \equiv \Psi_1(\mathbf{r})$  are referred here to as the "ground state" eigenvalue and eigenfunction.

In the close vicinity of the bifurcation point one can obtain the asymptotically-exact, overcritical solution of Eq. (22) in the form of a series in terms of two small parameters: the amplitude,  $\xi$ , and the "distance" from the bifurcation point,  $\alpha - \alpha_*$ . The bifurcation theory [68] ensures, however, that its main term always takes the form:

$$\eta(\mathbf{r}) \approx \xi\Psi_*(\mathbf{r}) + O(\xi^3) \quad (24)$$

Here,  $\xi$  is the amplitude to be determined from the nonlinear equation (22). This can be done in several ways. Making use of (23) and substituting the main term of the solution (24) one can, for example, represent (22) in the form:  $\xi \times [\hat{L}(\alpha) - \hat{L}(\alpha_*)]\Psi_* = \hat{N}(\xi\Psi_*)$ . Multiplying scalarly its both parts by  $\Psi_*$  one finds:

$$\left\langle \left[ \hat{L}(\alpha) - \hat{L}(\alpha_*) \right] \Psi_*, \Psi_* \right\rangle \xi = \left\langle \hat{N}(\xi\Psi_*), \Psi_* \right\rangle \quad (25)$$

where we use the notation:  $\langle f, g \rangle = \int f(\mathbf{r})g(\mathbf{r})d\Omega$  for the scalar product of two functions,  $f(\mathbf{r})$  and  $g(\mathbf{r})$ , in the Hilbert space. (25) referred to as a "branching equation" [68], represents a nonlinear equation with respect to  $\xi$ , only valid if  $\xi$  is small. Its solution yields the amplitude  $\xi$ , thus, giving simultaneously the solution (24) of the bifurcation problem valid in the close vicinity of the bifurcation point. Full details, theorems and their proofs one can find in the book of Vainberg and Trenogin [68].

We would like to stress, that though the above recipe heavily involves the solution of the linear equation (23), it represents in fact the solution of the nonlinear equation (22).

## 3.3 The process zone embedded into the mother phase

### 3.3.1 The bifurcation condition

Let us assume  $\alpha > 0$  and look for the point of instability of the trivial solution  $\eta = 0$  describing the homogeneous mother phase. It can be done using Eq. (18) within the approach formulated in the previous Section.

The correspondence between (22) and (18) is established as follows:

$$\hat{L}(\alpha)\eta = g\Delta\eta + \kappa V \frac{\partial\eta}{\partial x'} - \left[ \alpha \pm B \frac{\cos(\theta)}{\sqrt{r'}} \right] \eta = 0 \quad (26)$$

$$\hat{N}(\eta) = \beta\eta^3 \quad (27)$$

Let us now apply the above recipe of the bifurcation theory [68] to the case at hand. First of all one finds that at  $k > 0$  (corresponding to the sign "+") equation (23) has no discrete spectrum meaning that the solution  $\eta = 0$  of the equation (18) is stable at  $\alpha > 0$ .

In contrast to that, at  $k < 0$  (the sign "-") Eq. (23) has a discrete spectrum at  $\alpha > 0$  implying that Eq. (18) exhibits an instability. Let us consider the latter case.

At large value of  $\alpha$  equation (18) has the trivial solution  $\eta = 0$ . Below the bifurcation point one finds a non-trivial solution  $\eta = \eta(\mathbf{r}) \neq 0$  and  $\sigma_{ik}(\mathbf{r}) = \sigma_{ik}^{(0)}(\mathbf{r}) + O(\eta^2)$ , where  $\eta$  is small. According to its definition (7)  $\alpha$  is expressed in terms of temperature:  $\alpha = a(T - T_c)$ . Equation (36) yields, thus, the temperature,  $T_*$ , of LPT at the crack tip. The exact solution of the equation (23) with  $\hat{L}(\alpha)$  given by (26) is given in the next Section.

### 3.3.2 Exact results for the eigenvalue and eigenfunctions of Eq. (26)

Solution of (23) plays as we see an outstanding role defining both the bifurcation point,  $\alpha_* = \alpha_1$ , and the overcritical solution, (24) of the nonlinear equation (22). Let us solve it.

The linear part of equation (18) takes the form:

$$\begin{cases} g\Delta\Psi_n + \kappa V \times \partial\Psi_n/\partial x - \left[ \alpha_n - B \frac{\cos(\theta/2)}{r^{1/2}} \right] \Psi_n = 0; \\ \Psi_n(\infty) = 0; \quad |\Psi_n| < \infty \end{cases} \quad (28)$$

Making the substitution:

$$\Psi_n(\mathbf{r}) = \exp\left(-\frac{\kappa V}{2g}x\right) \times \psi_n(\mathbf{r}) \quad (29)$$

one proceeds to the equation in terms of  $\psi_n(\mathbf{r})$ :

$$g\Delta\psi_n - \left[ \alpha_n + \frac{\kappa^2 V^2}{4g} - B \frac{\cos(\theta/2)}{\sqrt{r}} \right] \psi_n = 0 \quad (30)$$

The parameter

$$R_1 = \left(\frac{g}{B}\right)^{2/3} = \frac{\pi^{1/3}}{2} \left[ \frac{g}{a|k|(1+\sigma)K_I} \right]^{2/3} \quad (31)$$

fixes the characteristic size of the distribution. Passing to dimensionless cylindrical coordinates  $\theta$  and  $\rho = \mathbf{r}/R_1$  one transforms (30) into the following equation:

$$\frac{\partial^2\psi_n}{\partial\rho^2} + \frac{1}{\rho}\frac{\partial\psi_n}{\partial\rho} + \frac{1}{\rho^2}\frac{\partial^2\psi_n}{\partial\theta^2} - \left( \lambda_n - \frac{\cos(\theta/2)}{\sqrt{\rho}} \right) \psi_n = 0 \quad (32)$$

where  $\lambda_n$  ( $n = 1, 2, \dots$ ) represents the eigenvalues of (32). They are related to  $\alpha_n$  as follows:

$$\lambda_n = \frac{g^{1/3}}{B^{4/3}} \left( \alpha_n + \frac{\kappa^2 V^2}{4g} \right) \quad (33)$$

Eq. (32) represents a 2D Schrödinger equation with an anisotropic potential  $U(\rho, \theta) = -\cos(\theta/2)/\sqrt{\rho}$  shown in Fig. 2.

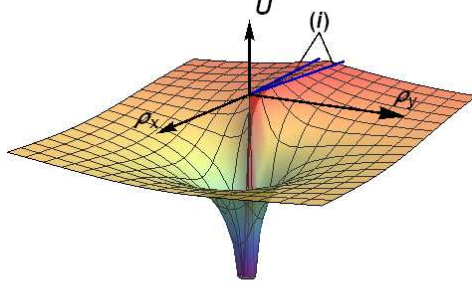


Figure 2: Potential  $U(\rho, \theta) = -\cos(\theta/2)/\rho^{1/2}$  of the Schrödinger equation (32). Here  $\rho_x = x/R$  and  $\rho_y = y/R$ . (i) indicates the position of the crack tip.

Let us look for the solution of Eq. (32) in the form  $\Psi(\rho, \theta) = \exp(-\varepsilon z)f(z)$ , where  $z = \rho^{1/2} \cos(\theta/2)$ . This yields the equation:

$$f''(z) - 4\varepsilon z f'(z) - 4(\varepsilon - z)f(z) = 0$$

Making use of the transformation  $f = \varphi(\zeta) \exp(z/\varepsilon)$  with  $\zeta = (z - 1/4\varepsilon^2)(\varepsilon/2)^{1/2}$  brings one to the equation in terms of  $\varphi$ :

$$\varphi''(\zeta) - 2\zeta\varphi'(\zeta) + m\varphi(\zeta) = 0; \quad m = 2[1 - (4\varepsilon^3)^{-1}] \quad (34)$$

The latter represents a Hermitian equation with the eigenvalue  $m$  only taking non-negative, integer, even values:  $m = 0, 2, 4, \dots$ . Using (34) one finds that the condition  $\varepsilon > 0$  only fulfills for the ground state solution  $m = 0$  yielding  $\varepsilon = 2^{-2/3}$  and  $\varphi(\zeta) = \text{const}$ . Now one can return to the initial variables and write down the solution of the equation (32) corresponding to  $m = 0$ :

$$\lambda_1 = \frac{1}{2\sqrt[3]{2}} \approx 0.397; \quad \psi_1(\rho) = \exp \left\{ -\frac{\rho}{\sqrt[3]{4}} + \sqrt[3]{4}\sqrt{\rho} \cos(\theta/2) \right\} \quad (35)$$

The latter is shown in Fig. 5 (A). Using (33, 35) one finds the ground state eigenvalue,  $\alpha_*$ :

$$\alpha_* = \frac{1}{2\sqrt[3]{2}} \frac{B^{4/3}}{g^{1/3}} - \frac{\kappa^2 V^2}{4g} \quad (36)$$

yielding finally the ground eigenvalue (37) and the eigenfunction (38).

### 3.4 The process zone embedded into the mother phase

#### 3.4.1 Bifurcation point

The above solution is valid at  $k < 0$ . It gives the ground state eigenvalue:

$$\alpha_{*1} = a(T_{*1} - T_c) = \frac{2^{2/3}}{\pi^{2/3} g^{1/3}} [a|k|(1 + \sigma)K_I]^{4/3} - \frac{\kappa^2 V^2}{4g} \quad (37)$$

and the eigenfunction:

$$\Psi_{*1}(\mathbf{r}) = \exp \left[ -\frac{\nu_1}{\sqrt[3]{4}} \frac{r}{R_1} \cos(\theta) - \frac{r}{\sqrt[3]{4}R_1} + \sqrt[3]{4} \sqrt{\frac{r}{R_1}} \cos(\theta/2) \right] \quad (38)$$

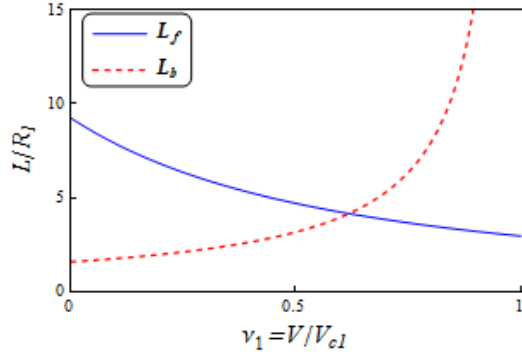


Figure 3: Dependence of  $L_f$  (solid line) and  $L_b$  (dashed line) upon  $\nu_1$ .

where  $\nu_1 = V/V_{c1}$  is the dimensionless velocity, and the critical velocity  $V_{c1}$  is defined as

$$V_{c1}(K_I) = \frac{2^{4/3} g^{1/3}}{\pi^{1/3} \kappa} [a |k| (1 + \sigma) K_I]^{2/3} \quad (39)$$

Its physical sense will be discussed below.

Let us note that Eq. (37) yields the case  $T_{*1} - T_c > 0$  shown in Fig. 1 (B).

Assigning the exponent to  $-1$  one finds the size,  $L_f$ , of the order parameter distribution in front of the tip:

$$L_{f1} = 2^{2/3} \frac{(3 + \nu_1) + 2 \times (2 + \nu_1)^{1/2}}{(1 + \nu_1)^2} R_1 \quad (40)$$

At the tip of the motionless crack ( $\nu_1 = 0$ ) one finds the order parameter distribution size  $L_{f1} \approx 9.25 R_1$  decreasing down to  $L_{f1} \approx 2.96 R_1$  at  $\nu_1 = 1$ . The dependence  $L_{f1} = L_{f1}(\nu_1)$  is shown in Fig. 3.

### 3.4.2 The overcritical solution

Substituting the obtained eigenfunction (38) as well as (26) and (27) into the branching equation (25) one obtains

$$I_2 (\alpha - \alpha_{*1}) \xi + I_4 \beta \xi^3 = 0 \quad (41)$$

where the factors  $I_n$  ( $n = 2, 4$ ) are the integrals over the whole plane:

$$I_n(\nu_1) = \int \Psi_*^n(\rho, \nu_1) d^2 \rho \quad (42)$$

depending upon  $\nu_1$ .

It should be noted that substitution of (24, 38) into the effective free energy, (17) yields the LPT free energy:

$$F_{\text{eff}} = F_0 + R_1^2 \left[ \frac{I_2 (\alpha - \alpha_{*1})}{2} \xi^2 + \frac{I_4 \beta}{4} \xi^4 \right] \quad (43)$$

As expected, its minimization with respect to  $\xi$  brings one back to the branching equation (41) giving the alternative way to build the overcritical solution.

The solution of the branching equation has the form:

$$\xi = \begin{cases} 0, & \alpha > \alpha_{*1} \\ \pm \left( \frac{I_2}{I_4} \right)^{1/2} \left( \frac{\alpha_{*1} - \alpha}{\beta} \right)^{1/2}, & \alpha \leq \alpha_{*1} \end{cases} \quad (44)$$

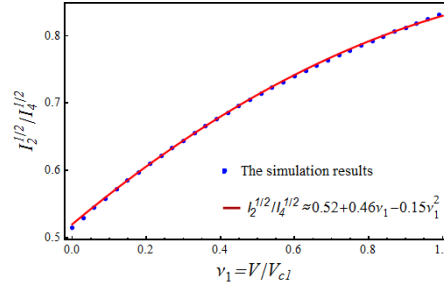


Figure 4: The ratio  $I_2^{1/2}/I_4^{1/2}$  obtained numerically as the function of the dimensionless velocity  $\nu$  and its fitting by the polynomial (45).

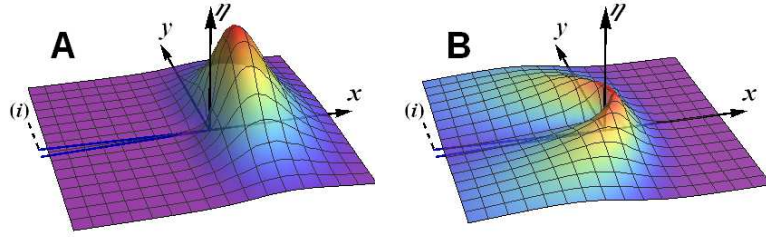


Figure 5: Spatial distribution of the order parameter,  $\eta(x, y)$ , in the vicinity of the motionless (A) and propagating (B) crack. Two blue lines (i) indicate the crack tip position.

The integrals  $I_n(\nu_1)$  cannot be obtained analytically at  $\nu_1 \neq 0$ . We calculated their ratio numerically by using a standard NIntegrate routine of Mathematica 10.1 [70] employing the even-odd subdivision method with the local adaptive strategy.

The ratio  $I_2^{1/2}/I_4^{1/2}$  obtained this way is shown in Fig. 4 versus the dimensionless velocity  $\nu_1$ . The numerical result can be accurately fitted by a simple polynomial:

$$\left(\frac{I_2}{I_4}\right)^{1/2} \approx 0.52 + 0.46\nu_1 - 0.15\nu_1^2 \quad (45)$$

Thus, the asymptotically exact overcritical solution (24) is obtained.

### 3.4.3 The critical velocity

The result (44) implies that the LPT only takes place at  $\alpha < \alpha_*$ , while at  $\alpha > \alpha_*$  the crack tip is undressed. Since at  $\alpha < 0$  the whole bulk of the solid transforms into the phase  $\eta \neq 0$ , the domain in which LPT takes place is restricted to the interval:  $0 < \alpha \leq \alpha_*$ . The latter result has a very important consequence. Making use of Eq. (36) one finds that at,  $V = V_{c1}$  the LPT disappears. In other words the LPT can only exist at the crack tip at  $V < V_{c1}$ , while at  $V \geq V_{c1}$  it vanishes. This property is fundamental for any LPT, both of the second and of the first order. It is a direct consequence of the fact that the order parameter has its own dynamics exhibiting an intrinsic characteristic time, and that as soon as  $V \geq V_{c1}$  the order parameter in front of the crack tip has no time to evolve from  $\eta = 0$  to  $\eta \approx \xi$ .

The spatial distribution of the order parameter (24) is shown in Fig. 5. Here (A) shows the order parameter in the vicinity of the motionless crack tip, while (B) displays that in the case of a propagating crack. This image is obtained with the velocity value  $V = 0.5V_{c1}$ .

One finds that the order parameter is highly localized in the vicinity  $r \lesssim 10R_1$  of the tip of the motionless crack. In the case of the moving crack tip (Fig. 5 B) the order parameter distribution is compressed in front of the tip and stretched in its back with respect to that at the motionless one. The length,  $L_b$ , of the order parameter distribution behind the tip of the propagating crack takes the form:

$$L_b = \frac{\sqrt[3]{4}R_1}{1 - V/V_{c1}} \quad (46)$$

Behind the crack the length,  $L_b$ , diverges, if  $V \rightarrow V_{c1}$  (Fig. 3). It should be noted that at  $V \rightarrow V_{c1}$  the amplitude,  $\xi$ , vanishes.

Let us summarize the results of the present Section. We have shown that in a solid with a crack the trivial solution  $\eta \equiv 0$  is stable at high temperatures ( $T > T_c$ ), but loses its stability at the point  $\alpha = \alpha_{*1} > 0$  corresponding to a temperature  $T_{*1}$  somewhat higher than that of the bulk phase transition:  $T_{*1} > T_c$ . This solution describes a region of the phase  $\eta \neq 0$  embedded into the matrix  $\eta \equiv 0$  representing the transformational PZ at the crack tip. In terms of temperature its existence is limited to the domain  $T_c < T < T_{*1}$ , while in terms of velocity to  $0 \leq V \leq V_{c1}$ . The transformational PZ at the tip of the propagating crack is deformed with respect to that of the motionless crack: the order parameter distribution is compressed in its front, while stretched in its back.

### 3.5 The process zone embedded into the daughter phase

Let us first find a solution for  $\eta(\mathbf{r})$  in the low-temperature phase ( $\alpha < 0$ ). We will assume in addition that  $|\alpha|$  is large enough, so that where this solution is stable. Observing that at  $r \gg (g/\alpha)^{1/2}$  the terms  $\sim \Delta\eta$  and  $\sim \partial\eta/\partial x$  in (18) are much smaller than the others and neglecting them, one finds the approximate distribution  $\eta = \eta_0(\mathbf{r})$  in the daughter phase:

$$\eta_0(r, \theta) \approx \frac{1}{\beta^{1/2}} \left( -\alpha - B \frac{\cos(\theta/2)}{\sqrt{r}} \right)^{1/2} \quad (47)$$

To be specific, from two solutions of the equation of state we have chosen a positive one. Let us now look for the solution perturbation in the form:  $\eta(\mathbf{r}) = \eta_0(\mathbf{r}) + \delta\eta(\mathbf{r})$ . Substituting it into (18) one finds that the term  $\delta\eta(\mathbf{r})$  is subjected to the equation (22) with

$$\hat{L}(\alpha)\delta\eta = g\Delta\delta\eta + \kappa V \frac{\partial\delta\eta}{\partial x} - \left[ 2|\alpha| \mp B \frac{\cos(\theta)}{\sqrt{r}} \right] \delta\eta \quad (48)$$

and

$$\hat{N}(\delta\eta) = 3 \left( -\alpha\beta - \frac{B\beta \cos(\theta/2)}{\sqrt{r}} \right)^{1/2} \delta\eta^2 + \beta\delta\eta^3 \quad (49)$$

In this case at  $k < 0$  (the sign "+" in 48) equation (48) appears to have no discrete spectrum implying that the solution (47) is stable. The discrete spectrum indicating the instability, however, exists at  $k > 0$  (the sign "-" in 48). Below we consider this latter case.

Applying the analysis already described above to the present case one finds the eigenfunction (38), in which instead of  $R_1$  one should take a characteristic size  $R_2$  expressed as:

$$R_2 = \left( \frac{g}{2B} \right)^{2/3} = \frac{\pi^{1/3}}{2^{5/3}} \left[ \frac{g}{akK_I(1 + \sigma)} \right]^{2/3} \quad (50)$$

which is smaller than (31) by the factor  $2^{-2/3}$ . The bifurcation point has the form:

$$\alpha_{*2} = -\frac{1}{2^{1/3}\pi^{2/3}g^{1/3}} [ak(1 + \sigma)K_I]^{4/3} + \frac{\kappa^2 V^2}{8g} \quad (51)$$

such that a non-trivial solution  $\delta\eta(\mathbf{r}) = \xi_2\Psi_*(\mathbf{r})$  takes place at  $0 \geq \alpha \geq \alpha_{*2}$  corresponding to the phase diagram shown in Fig. 1 (A). Its amplitude,  $\xi_2$ , should be determined from the branching equation. Analogously to the previous case the relation (51) gives rise to the critical velocity:

$$V_{c2} = \frac{2^{4/3}g^{1/3}}{\pi^{1/3}\kappa} [akK_I(1 + \sigma)]^{2/3} \quad (52)$$

limiting the existence of the high-temperature PZ in the matrix of the low-temperature phase. The latter is by the factor of  $2^{2/3}$  larger than  $V_{c1}$ .

Since the overcritical solution (24) for  $\delta\eta$  is determined by the same eigenfunction (38) as that for the high-temperature case, the distribution,  $\delta\eta(\mathbf{r}) = \xi_2\Psi_*(\mathbf{r})$  has the same form as that of the order parameter in the high-temperature PZ. The distribution is shown in Fig. (5). Analogously to the high-temperature case the distribution,  $\delta\eta(\mathbf{r})$ , at the tip of the propagating crack is compressed in its front, stretched backwards and the relation (46) holds. The amplitude,  $\xi_2$ , should be determined from the branching equation.

These further results are easy, but rather cumbersome to derive, and we, therefore, give the calculations in Appendix C.

Let us summarize the findings of this Section. We found that the inhomogeneous solution  $\eta_0(\mathbf{r})$  describing the order parameter distribution in the low-temperature phase is stable at  $\alpha < \alpha_{*2} < 0$ . At  $\alpha = \alpha_{*2} < 0$  this solution becomes unstable and the solution,  $\eta_0(\mathbf{r}) + \delta\eta(\mathbf{r})$ , branches decreases off from  $\eta_0$ , the signs of  $\eta_0$  and  $\delta\eta$  being different. This means that the zone with the high-temperature phase,  $\eta \equiv 0$ , emerges at the crack tip at  $\alpha = \alpha_{*2}$  and exists within the domain  $0 \leq \alpha \leq \alpha_{*2}$  and at  $0 \leq V \leq V_{c2}$ .

## 4 Simulation

### 4.1 Rescaling

Based on the bifurcation theory our analytical results are only valid in the close vicinity of the bifurcation point. To study the problem far from the bifurcation we simulated solution of the equation (18). We report below the simulation of the daughter phase PZ embedded into the matrix of the mother phase.

The equation (18) has been rescaled making the variables dimensionless and minimizing the control parameters number:  $x \rightarrow d_1x_1$ ,  $y \rightarrow d_1y_1$  and  $\eta(x, y) \rightarrow d_2u(x_1, y_1)$  with the scaling factors  $d_1 = R_1$  and  $d_2 = B^{2/3}/g^{1/3}\beta^{1/2}$ . The rescaled equation (18) takes the form:

$$\Delta_1 u + 2^{1/3}\nu \frac{\partial u}{\partial x_1} - \left[ q - \frac{\cos(\theta/2)}{r_1^{1/2}} \right] u - u^3 = 0 \quad (53)$$

where  $\Delta_1 = \partial^2/\partial x_1^2 + \partial^2/\partial y_1^2$ ,  $r_1 = (x_1^2 + y_1^2)^{1/2}$ ,  $d\Omega_1 = dx_1 dy_1$  and the dimensionless parameter  $q$  is expressed as follows:

$$q = \frac{g^{1/3}}{B^{4/3}}\alpha$$

Let us note that in terms of the rescaled parameters  $(q, \nu)$  the analytical expression for the bifurcation condition (37) takes the form

$$q_c = \frac{1 - \nu^2}{2 \times 2^{1/3}} \quad (54)$$

while the overcritical solution (38, 44) at  $q < q_c$  is expressed as:

$$u(r_1, \theta) = \left[ \frac{I_2(q_c - q)}{I_4} \right]^{1/2} \exp \left\{ -4^{-1/3}r_1 [1 - \nu \cos(\theta)] + 4^{1/3}r_1^{1/2} \cos(\theta/2) \right\} \quad (55)$$

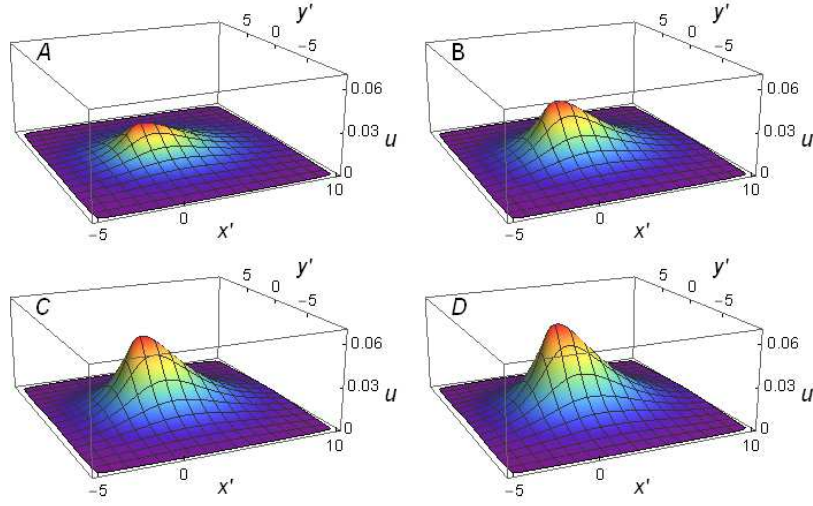


Figure 6: Order parameter distribution obtained by simulations at  $\nu = 0$  and various values of  $q_c - q$ : (A)  $1.5 \times 10^{-4}$ , (B)  $6.5 \times 10^{-4}$ , (C)  $12 \times 10^{-4}$  and (D)  $16 \times 10^{-4}$ .

## 4.2 Results

We used a pseudo-time stepping approach representing a version of the iteration method. Its description along with software technical details and settings are given in the Appendix C. The pseudo-time stepping approach converged away from the points:  $q = 0$  and  $q = q_c$  (54). In practice, we obtained a good convergence at  $q > 0.1$ , above the points of the global bifurcation. Closer to the point  $q = 0$  we were unable to get an equilibrium solution. In the vicinity to the point  $q = q_c$  the method produced a small regular error discussed in details below. Apart from that the method exhibited a good convergence, enabling us to study the distribution of the rescaled order parameter,  $u(x_1, y_1)$  in the vicinity of the crack tip.

Figure 6 shows the distributions of the rescaled order parameter at the tip of a motionless crack ( $\nu = 0$ ) at the successively increasing values of the difference  $q_c - q > 0$  below the bifurcation point. As expected the order parameter grows with  $q_c - q$ , its distribution being close to that described by Eq. (55) at  $\nu = 0$  (shown in Fig. 5 A).

To check the proximity of the simulated results to the analytical one we plotted the cross-sections of the above solutions by the plane  $(x_1, u)$  (Fig. 7). This has been done by sampling the solution points from the layer with the thickness 1.5 along the plane  $y_1 = 0$ . Because the simulation results exhibit a regular shift of the bifurcation point we plot the order parameter versus the distance from the bifurcation,  $q_c - q$ , rather than  $q$ . The solid lines in Fig. 7 show the cross-section of the analytical solution (55) at the same values of  $q_c - q$ . One can see that close to the bifurcation point the solution obtained by the simulation is rather close to the analytical one (Fig. 7).

The distribution of the rescaled order parameter,  $u(x_1, y_1)$  at the tip of the propagating crack ( $\nu_1 \geq 0$ ) at the same value of  $q$  is shown in Fig. 8. One can see that the crack motion transforms the distribution in several ways. First, with the increasing of the dimensionless velocity,  $\nu_1 = V/V_{c1}$ , it becomes lower and vanishes as soon as the velocity achieves the bifurcation line. Besides, the order parameter distribution is compressed in front of and stretched out behind the tip with respect to that at the tip of the motionless crack.

The latter is in line with the predictions of the analytical solution (55) at  $x_1 < 0$ ,  $y_1 = 0$ :

$$u(x_1, 0) \sim \exp \left[ -4^{-1/3} x_1 (1 - \nu) \right]; \quad x_1 < 0 \quad (56)$$

describing the distribution behind the crack tip. The distribution length diverges as  $4^{1/3}/(1 -$

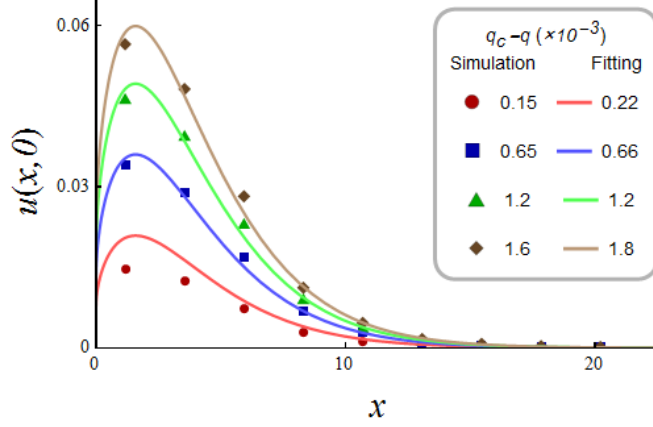


Figure 7: Cross-section of the order parameter distribution along the plane  $y = 0$  shown at  $x > 0$  corresponding to  $\nu = 0$  and various values of  $q$ . Dots show the simulation results at different values of  $q_c - q$ , while the solid line display their fittings with the expression (55). The legend for the dots indicate the  $q$  values used in the simulation, while that for the solid lines yields  $q$  values obtained by the fitting.

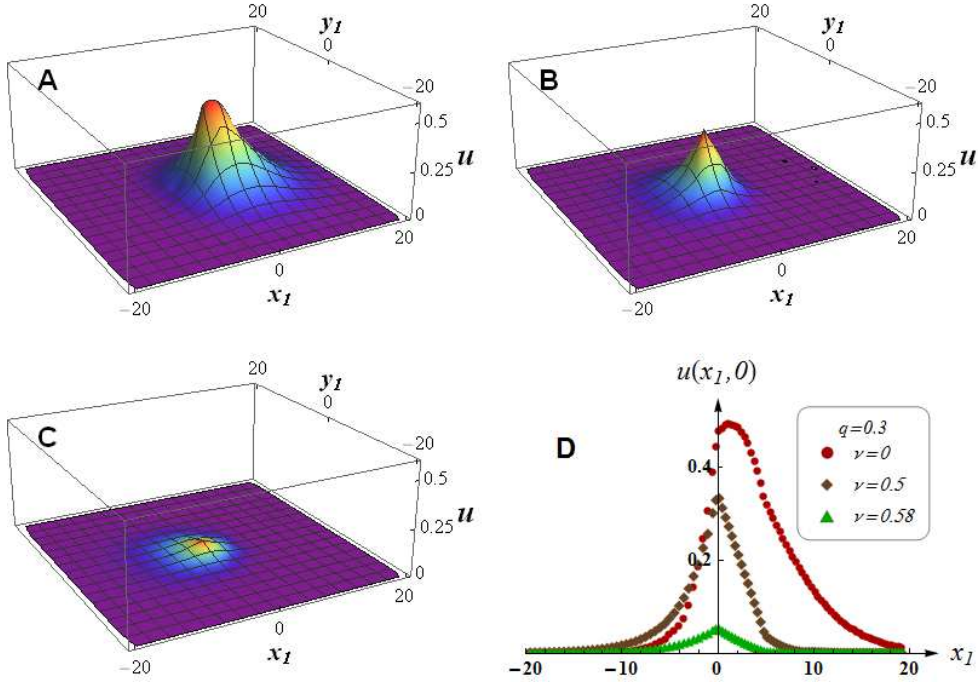


Figure 8: Order parameter distribution in the vicinity of the tip of the crack propagating in the positive direction of  $x$  along the line  $y = 0$ . All images have been obtained by simulation with  $q = 0.3$ . (A) shows the motionless case  $\nu = 0$ , while (B) and (C) display the case of the propagating crack:  $\nu = 0.5$  (B) and  $\nu = 0.58$  (C). The image (D) shows the cross-section of the distributions shown in (A-C) by the plane  $y = 0$ .

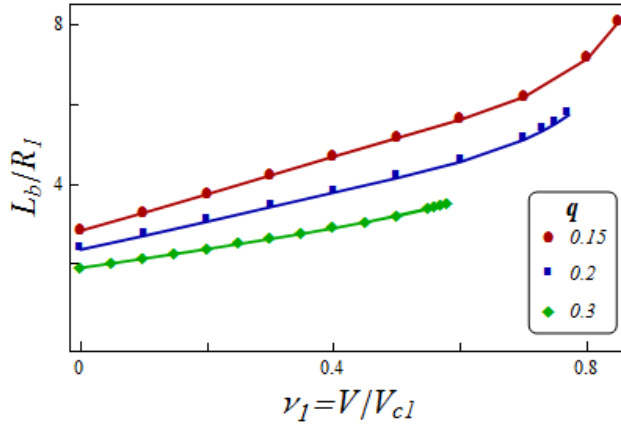


Figure 9: Dependence of the dimensionless length,  $L_b/R_1$ , of the order parameter trail upon the dimensionless velocity,  $\nu_1 = V/V_{c1}$  for several values of the parameter  $q$ . For each value the data has been taken until the bifurcation line has been approached. Dots show the simulation result, while the solid line is guiding the eye.

$\nu$ ) as  $\nu \rightarrow 1$  (see also 46). The simulation, indeed, looks close to the exponents (Fig. 8 D). To check this we fitted the backward part of the distributions by the exponents  $u(x_1 < 0, 0) \sim \exp(x_1 R_1/L)$ . Figure 9 displays the dependence of  $L/R_1$  upon  $\nu_1$  at different values of the control parameter  $q$  obtained by the simulations.

It should be noted that the trail length, indeed, increases with the velocity, but does not follow the behavior (46) predicted by our analytical approach. This is because the analytical prediction is only valid very close to the bifurcation point, which is not the case for most of the points shown in Fig. 9.

The plane  $(\nu_1, q)$  is divided into two regions. In the region I ( $q < q_c$ ) the transformational PZ at the crack tip exists, while it vanishes at the boundary ( $q = q_c$ ) and does not exist in the region II ( $q \geq q_c$ ). To check this we made simulations by fixing the value of  $\nu_1$  and evaluating the maximal order parameter value,  $u_{\max}$ , at different  $q$  points. One can see that at large  $q$  values  $u_{\max}$  vanishes, while emerging after a certain threshold.

The values of these threshold have been extracted from the above data by fitting to the function:

$$u_{\max}(q) = \begin{cases} 0, & q > q_{cn} \\ u_0 (q_{cn} - q)^{1/2}, & q \leq q_{cn} \end{cases} \quad (57)$$

where  $u_0$  and  $q_{cn}$  are the fitting parameters, and  $q$  is the variable. The parameter  $q_{cn}$  represents, therefore, the bifurcation value obtained from the simulations. The subscript "n" stays for "numeric", to distinguish  $q_{cn}$  from the analytically obtained bifurcation boundary,  $q_c$ . The dynamic phase diagram obtained this way is shown in Fig. (11).

One can see that the simulation gives the values of the boundary points that are regularly shifted over about 5% upwards with respect to the line obtained analytically. We did not succeed to obtain values close to the line  $q_c(\nu)$ . This is due to the singularity  $\sim r^{-1/2}$  in the equation (53) [69].

## 5 Discussion

### 5.1 Our findings

We formulated a natural approach to describe the LPT at the tip of the crack taking into account the order parameter, the internal degree of freedom responsible for the phase transi-

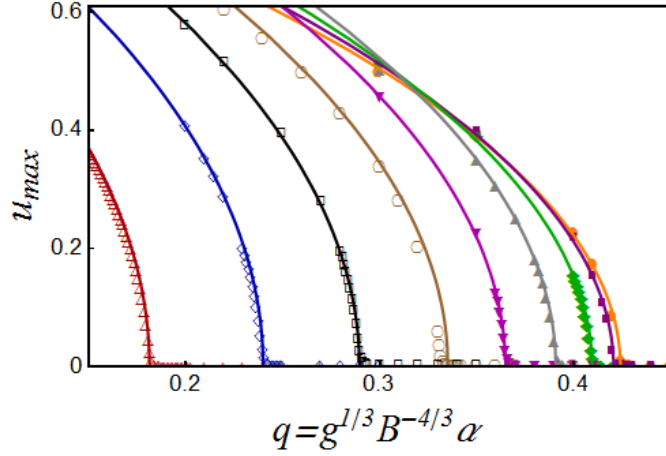


Figure 10: Dependence of the maximum value of the rescaled order parameter,  $u_{\max}$ , upon the control parameter  $q$  at different values of the dimensionless velocity  $\nu_1$ : disks show  $\nu_1 = 0$ , squares - 0.1, filled diamonds - 0.2, filled vertex-up triangles - 0.3, vertex-down triangles - 0.4, open circles - 0.5, open squares - 0.6, open diamonds - 0.7, open vertex-up triangles - 0.8. The solid lines show their fitting to the function (57).

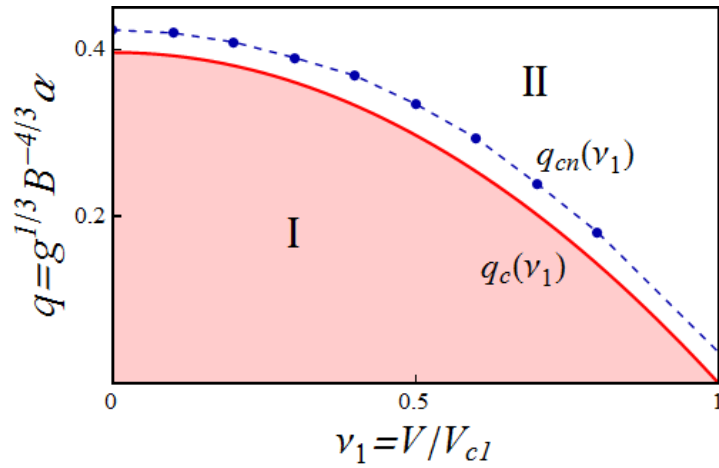


Figure 11: Dynamic phase diagram divides the  $(\nu_1, q)$  plane into the part I in which the transformational process zone is present at the crack tip and II without the zone. The dots show the results of simulation. They are connected by a dashed line to guide the eye. The solid line shows the theoretical boundary given by the expression (54).

tion. The LPT takes place as the response of the solid to the local stress inhomogeneity. This suggests that any type of stress concentrator may generate LPT. In addition to the crack tips the role of such stress concentrators play surfaces, inclusions, grain and twin boundaries, dislocations and disclinations. It is, further, clear that for any of this type of the concentrators the LPT (i) decreases the total concentrator energy and (ii) introduces its dissipation in the process of motion, thus, influencing its static [48], [49] and dynamic [37] properties.

Among the LPT generating stress concentrators cracks are the most powerful ones. LPT-induced variation of the cracks properties may considerably alter the ability of material to resist fracture. This paper focuses on the LPT at the crack tips. The conclusions of the present paper are based on our following fundamental findings.

First, we have found the exact solution for the point of bifurcation both in the case of the motionless and propagating crack.

Second, we established the existence of the critical crack velocity controlling the disappearance of the LPT zone at high speeds.

Third, we have found an analytical, asymptotically exact solution of the nonlinear equation describing the order parameter distribution close to the bifurcation point.

Fourth, by numeric simulation we obtained the solutions away from the bifurcation point which is in line with our analytic solution.

It should be mentioned here that the present results will be further used for analysis of the fast crack propagation published separately.

## 5.2 Effect on the crack behavior of the second versus the first order transitions

In this paper we only addressed the phase transitions of the second order. Second order phase transitions are generally considered to be soft. This opinion gives rise to the illusion that they should only have a negligible effect on the crack dynamics. This point of view is erroneous. The softness of the second order phase transitions only means that the solid continuously passes from the state  $\eta = 0$  to the state  $\eta \neq 0$  in the transition or bifurcation point. This is in contrast to the first order transitions where in the transition point the order parameter exhibits a jump. The effect of the LPT on the crack dynamics is, however, not related to the order parameter behavior in the transition point. It depends upon absolute values the order parameter can achieve within the LPT zone. In the discussion below we will argue that the zone is typically very wide. This implies that the PZ order parameter is most often in the saturated state. In this respect the second order phase transition exhibits no qualitative difference from that of the first order. In the case of structural phase transitions the order parameter can be constructed using the atoms displacements from their positions in the mother phase. Their saturation values may achieve the values smaller, but comparable to the crystal lattice cell dimensions both in the case of the first and second order phase transition.

It should be, further, noted that for one thing the value of the bifurcation point,  $T_*$ , is obtained by the analysis of the linear part, (23), of the nonlinear equation for the order parameter. For the other, the answer to the question, whether the PT is of the second, or first order depends only upon the structure of the nonlinear terms of the free energy (7). This suggests that the result (2) for  $T_*$  is valid both for the cases of the first and second order transitions. Here we take this assumption as granted. A rigorous proof of this statement will be published elsewhere.

Table 1: Material constants of BaTiO<sub>3</sub>, PbTiO<sub>3</sub> and LiNbO<sub>3</sub>

	BaTiO <sub>3</sub>				PbTiO <sub>3</sub>	LiNbO <sub>3</sub>
$a$ ( $\times 10^{-4}$ K <sup>-1</sup> )	2.1 [71]				2 [71]	0.7 [76]
$g$ ( $\times 10^{-16}$ cm <sup>2</sup> )	1 [86]				1 [86]	0.3 [72]
$K_{IC}$ ( $\times 10^8$ erg cm <sup>-5/2</sup> )	0.6 ÷ 2.0 [73]				1.4 [89]	1 [79]
$\kappa$ ( $\times 10^{-14}$ s)	1 [80]				1 [81]	-
$T_m$ (K)	1898 [83]				1443 [84]	1526 [85]
$T_0$ (K)	II-III 394	III-IV 284	IV-V 200	[88]	850 [88]	1460 [82]
$k$ ( $\times 10^{-8}$ K cm <sup>3</sup> erg <sup>-1</sup> )	-0.8	-0.3	-0.1	[88]	-1 [74]	0.018 [72]

### 5.3 Estimates

#### 5.3.1 Material parameters and results for selected materials

The temperature shift value,  $\Delta T_*$ , is of a great importance, since it determines the phase diagram region where the PZ influences the crack behavior. It is interesting, therefore, to have numerical values of  $\Delta T_*$  at least for some materials. As the examples let us consider ferroelectrics BaTiO<sub>3</sub>, PbTiO<sub>3</sub> and LiNbO<sub>3</sub>.

All the three materials belong to a large family of perovskites, LiNbO<sub>3</sub> exhibiting a distorted perovskite structure [82].

The high-temperature phases of PbTiO<sub>3</sub> and BaTiO<sub>3</sub> exhibit a cubic symmetry. The cubic phase in PbTiO<sub>3</sub> exists above 850 K, while transforming into the tetragonal one at lower temperatures [74]. In contrast to that BaTiO<sub>3</sub> exhibits the cubic phase (II), tetragonal (III), rhomboherdic (IV) and orthorhombic phase (V). The numeration of the phases is given according to [88]. The phase diagram of BaTiO<sub>3</sub> can be found in the paper [75]. All the transitions of BaTiO<sub>3</sub> and PbTiO<sub>3</sub> are of the first order.

The Landau theory enables one to describe possible transitions in the both materials as generated by the symmetry lowering of the cubic mother phase, the order parameter being a 3D vector,  $(\eta_1, \eta_2, \eta_3)$  associated with the polarization. In the cubic phase  $\eta = (0, 0, 0)$ . In all the low-temperature phases showing up in the phase diagrams the order parameter has only one independent component:  $(\eta, 0, 0)$  in the tetragonal,  $(\eta, \eta, \eta)$  in the rhombohedric, while the orthorhombic phase is described by  $(\eta, \eta, 0)$  [59]. Effectively, therefore, the problem is reduced to a single order parameter enabling one to directly apply the approach developed in the present paper. It should be noted that the free energy of BaTiO<sub>3</sub> and PbTiO<sub>3</sub> has striction terms giving rise to nondeviatoric spontaneous strain in addition to the deviatoric one. For the order of magnitude estimate done below this difference is, however, irrelevant.

LiNbO<sub>3</sub> possesses the symmetry  $R\bar{3}c$  in the high-temperature paraelectric phase and exhibits a 2nd order transition into the ferroelectric  $R3c$  phase at 1460 K [82], the transition being described by a one-component order parameter.

Material parameters of BaTiO<sub>3</sub>, PbTiO<sub>3</sub> and LiNbO<sub>3</sub> are summarized in the Table 1.

Here  $T_m$  is the melting point. In the case of BaTiO<sub>3</sub> and PbTiO<sub>3</sub>  $T_0$  is the temperature of the first order transition, while for LiNbO<sub>3</sub> this value yields the Curie point. Note take the scatter of the  $K_{IC}$  values for BaTiO<sub>3</sub> (Table 1) originates from experimental results obtained on ceramics with different properties (such as porosity, grain size, etc.). It gives rise to the corresponding spread of the estimates for BaTiO<sub>3</sub> parameters summarized in Table 2. In the case of BaTiO<sub>3</sub> the last row yields the values of the phase transition line slopes corresponding to each its transition: II-III, III-IV and IV-V,

The estimates following from the above material constants are collected in Table 2.

In BaTiO<sub>3</sub> the slopes of all phase transition lines are negative. For this reason the

Table 2: Estimates of the LPT characteristics

	$\Delta T_*$ (K)	$\Delta T_*/T_m$	$L_f$ (nm)	$V_c$ ( $\times 10^6$ cm / s)
BaTiO <sub>3</sub> II-III	$10^3$ to $10^4$	1 to 10	0.1 to 1	1
BaTiO <sub>3</sub> III-IV	$10^2$ to $10^3$	0.1 to 1	1	0.1 to 1
BaTiO <sub>3</sub> IV-V	$10^2$ to $10^3$	0.1 to 1	1	0.1 to 1
PbTiO <sub>3</sub>	$10^3$	1	1	1
LiNbO <sub>3</sub>	30	0.01	10	-

transformation zones only show up above the corresponding transition lines. Thus, during fracture of the cubic BaTiO<sub>3</sub> one will find at the tip a zone containing the tetragonal phase III embedded into the cubic matrix II. The above estimates show that this zone exists up to the temperatures of at least  $\sim 100$  to  $\sim 1000$  K above the temperature  $T_{II-III} = 394$  K of the bulk phase transition.

The zone containing the orthorhombic phase IV embedded into the bulk tetragonal phase III should be found at the crack tip taking place above the bulk transition temperature  $T_{III-IV}$ . It should be especially noted that the temperature interval of existence of the orthorhombic zone,  $\Delta T_{*III-IV} \sim 100$  to  $1000$  K, is greater than the "distance" between the transitions II-III and III-IV:  $T_{II-III} - T_{III-IV} = 110$  K. Thus, the orthorhombic zone shows up in the whole region of existence of the tetragonal phase and will be detectable within the bulk cubic phase together with the tetragonal zone. In other words, a two-phase transformation zone should take place over the temperature  $T_{II-III}$ .

It is worth noting that the room temperature belongs to the temperature interval in which the tetragonal bulk phase III exists. It makes observation of the local phase transition phenomenon in the phase III of BaTiO<sub>3</sub> convenient.

Finally, the zone with the ferroelectric, rhomboedral phase V should take place on the background of the ferroelectric, orthorhombic, bulk phase IV up to  $\sim 100$  to  $1000$  K above the bulk transition temperature  $T_{IV-V}$ . One finds  $T_{IV} - T_V = 84$  K and  $\Delta T_{*IV-V} \gtrsim T_{IV} - T_V$ . This implies that the rhombohedral zone should be detectable within the whole domain of existence of the bulk, orthorhombic phase IV and as well as in the tetragonal matrix III. A proper description of such multiphase zones is, however, complex; we leave it for another paper.

Since in PbTiO<sub>3</sub> one finds  $k < 0$ , it only exhibits the transformation zone during fracture of the cubic phase (i.e. above the transition line of the phase diagram). From its phase diagram [74] one can see that at the atmospheric pressure the cubic phase only exists at the temperature over about  $T_0 \approx 850$  K. If the PbTiO<sub>3</sub> fracture takes at temperatures between  $T_0$  and about  $1000$  K above  $T_0$ , our estimates predict that it will be followed by formation of the tetragonal transformation zone at the crack tip embedded into the matrix of the cubic phase.

It should be noted that both in the case of BaTiO<sub>3</sub> and PbTiO<sub>3</sub> the ratio of the temperature shift,  $\Delta T_*$ , to the melting temperature,  $T_m$ , is between  $\sim 0.1$  and  $\sim 1$ . Since the whole phase diagram spans between  $0$  K and  $T_m$ , this shows that the region of the zone existence covers a considerable part of or even the whole phase diagram.

In principle, the slope,  $k$ , of the phase diagram line may have any value, including a very large or a small one. The latter is the case of LiNbO<sub>3</sub> where it gives rise to a relatively small shift of  $\sim 10$  K.

### 5.3.2 Typical values of the temperature shift $\Delta T_*$

It should be noted that the huge values of  $\Delta T_* \sim 100$  to  $1000$  K are not only inherent for BaTiO<sub>3</sub>, PbTiO<sub>3</sub>. To argue that let us note the expression (2) for the temperature shift at

$V = 0$  can be written as:

$$\Delta T_* \sim r_{c0}^{-2/3} (k K_{IC})^{4/3} \quad (58)$$

where  $r_{c0} = (g/a)^{1/2}$  is the order parameter correlation radius at the "distance" of 1 K from the transition line. The latter represents one of the most accessible parameters, since it can be extracted from the width of the X-ray spectrum peaks [87] typically exhibiting the value of  $r_{c0} \sim 1$  to  $10 \text{ nm K}^{1/2}$ , as well as that there is a typical value of the slope of the phase diagram line  $k \sim 1$  to  $10 \text{ K / kbar} \sim (0.1 \div 1) \times 10^{-8} \text{ K cm}^3 \text{ erg}^{-1}$  [88], and the typical value of the fracture toughness of the inorganic solids is  $K_{IC} \sim 1 \text{ MPa m}^{3/2} \sim 10^8 \text{ erg cm}^{-5/2}$  [90] one finds the typical temperature shift:

$$\Delta T_* \sim 10^2 \text{ to } 10^4 \text{ K}$$

Since the typical values of the melting point of inorganic solids is  $T_m \sim 10^3 \text{ K}$ , one concludes that  $\Delta T_*$  typically covers a considerable part, if not the whole phase diagram above or below the line of the bulk phase transition.

## 5.4 On difficulties and possibilities to detect a transformation process zone outside of the hysteresis region

In the introduction we listed a number of materials for which LPT observation has been reported. A relatively small number of such materials others than those of the martensite type seems to contradict our main findings. This is, however, only an apparent contradiction. Detailed inspection of the works cited above shows that in most of them the local phase transition has been detected by the analysis of the fracture surface available after the sample has been broken, the so-called, "post mortem" examination. In the case of the zirconia, for example, the fracture surface exhibited a layer of the monoclinic daughter phase about  $1 \mu\text{m}$  thick on top of the tetragonal mother phase surviving a considerable time after fracture. This requires the zirconia to be deep within the hysteresis region of its phase diagram. Indeed, martensitic transformations in both martensite-austenite metals and zirconia exhibit wide hysteresis regions. This is, however, rare, for most solids the hysteresis does not exceed  $\sim 10 \text{ K}$ , while the second order transitions have no hysteresis at all.

In contrast to the local phase transition within the hysteresis, the transformation zone outside of the hysteresis region is only present under stress. As soon as the stress is removed it immediately disappears. It cannot, therefore, be detected by the "post mortem" inspection of the fracture surface.

Further, at a high temperature one may observe no zone at  $K_I = K_{IC}$ , but since  $\Delta T_* \sim K_I^{4/3}$  the zone may show up at higher stress intensity factor, that is, at the tip of a propagating, rather than motionless crack.

Detection of a local phase transition outside the hysteresis region is, therefore, a challenging experimental task.

## 5.5 The crack tip zone concept

The notion "process zone" is already in use since long time. Its emergence reflects the understanding that the small domain in the immediate vicinity of the tip of a brittle crack should have special properties due to high stresses present there. Behavior of propagating cracks exhibits pronounced deviations from predictions of linear fracture mechanics [38]. It is generally believed that they can only be explained by mechanisms located within the process zone [40], [41]. Nevertheless, the content of this notion stays so far on an intuitive level. Below we outline the process zone concept from the physical point of view.

Equation of motion of the crack tip can be regarded as that of balance of forces, the driving force,  $K_I^2/E$ , being balanced by (i)  $K_{IC}^2/E$  representing a kind of "dry" friction force and (ii) by additional resistance force generated within the process zone. Within the force balance concept the zone is the source of resistance of the solid to the crack propagation, since it is here that this additional force is generated.

The concept of the process zone itself implies that it is possible to distinguish the solid inside from that outside of the zone using at least one physical property. Though in principle one can imagine a zone with a smooth, gradual variation of all its properties, we believe that the situation in which at least one physical property of the solid abruptly varies across the zone boundary is much more realistic and, hence, often met.

We parametrized the differences of the solid properties inside the zone from those outside by the field,  $\eta$ . Without the loss of generality we assume  $\eta = 0$  inside the zone, while vanishing outside. In this respect our point of view is akin to the popular phase field approach [91]. In principle, this field may describe either an abrupt quantitative variation of some solid property, or its qualitative change. In the latter case the situation is usually qualified as a phase transition, while  $\eta$  is referred to as the order parameter. In the present paper we focus on this latter case.

At present the terms "phase transition" and "order parameter" unify a crystal structure variation of solids with bifurcations in non-linear systems, both equilibrium and non-equilibrium, such as e.g., bifurcations taking place during chemical reactions [92]. It is tightly related to the fact that each of these transitions can be described by its inherent order parameter(s). They exhibit a few classes of universalities generating the corresponding types of kinetic equations imposed on the order parameter(s), therefore, giving rise to different configurational forces acting on the zone boundary and, hence, exerted on the crack tip. The most often met universality class is associated with the order parameter obeying the Ginzburg-Landau-Khalatnikov equation [92], since it is related to the simplest bifurcation. This one is addressed in the present paper. The zone at the crack tip may, however, be associated with any of such phase transitions or their combinations.

The long-wave elastic field at the tip of a brittle crack exhibits its own universal behavior expressed by the well-known small-scale approximation for the stress or strain field  $\varepsilon_{ii} \sim r^{-1/2}$ . This latter universality combines with one of those mentioned above.

We illustrate the above ideas within the example of classical structural phase transitions related to changes in lattice structures in crystals in response to the temperature and/or pressure variations. Structural phase transitions can be classified according to their own classes of universalities. These are related first of all to the symmetry change taking place during the transition(s) [58], [59], [60]. The latter is manifested in (i) the number of components of the order parameter and (ii) structure of the Ginzburg-Landau-Khalatnikov equation. It, in particular, defines the form of interaction of the order parameter with other degrees of freedom including elastic ones.

One observes in addition that the ranges of the values of material parameters in use are quite narrow. This allows one to determine typical numerical values of the parameters derived in our model.

To conclude, within our approach the process zone is regarded as a domain which is unambiguously different from the bulk of the solid. The difference may either be quantitative (such as a prominent variation of at least one physical parameter), or qualitative (e.g. the difference in its symmetry, crystal structure or chemical composition). Such a variation (or their combination) takes place due to the high stress in the vicinity of the crack tip, as a consequence of the nonlinearity. Our approach is, further, based on the accounting for the universalities inherent both to the fracture mechanics and bifurcations of non-linear systems offering a way to classify zones according to the universality classes as well as on

the observation of their typical features. The zones related to the elastic nonlinearity [43], formation of the secondary cracks [40], crack tip chemical reactions [93], electronic structure variation [94] as well as the transformation zone reported in the present paper fit into this general scheme.

## 6 Appendix A: Exclusion of the acoustic variables

Below we exclude acoustic degrees of freedom from the equation of motion as it has been proposed in the paper [48]. Making use of (12, 13) one can express the displacement vector,  $u_i$  as

$$u_i = u_i^{(0)}(\mathbf{r}) + A \int G_{ij}(\mathbf{r} - \mathbf{r}') \frac{\partial \eta^2(\mathbf{r}')}{\partial x'_j} d^2 x' \quad (59)$$

where  $u_i^{(0)}(\mathbf{r})$  is the displacement field created by the "undressed" crack (that is, the crack without any LPT) and  $G_{ij}(\mathbf{r})$  is the Green function of the elastic solid with a cut. To the best of our knowledge the explicit form of such a Green function is unknown. We approximate it with the Green function of the infinite elastically-isotropic body [66]. Passing to the reciprocal space under the integral in the representation (59) and making use of the identity

$$G_{ik}(\mathbf{q}) q_j q_k = \frac{1 - 2\sigma}{2\mu(1 - \sigma)} \frac{q_i q_j}{\mathbf{q}^2}$$

(where  $G_{ik}(\mathbf{q})$  is the Fourier-transform of the Green function) one finds the strain field,  $\varepsilon_{ik}(\mathbf{r})$  in the following form:

$$\varepsilon_{ik}(\mathbf{r}) = \varepsilon_{ik}^{(0)}(\mathbf{r}) + \frac{A(1 - 2\sigma)}{2\mu(1 - \sigma)} \int \frac{q_i q_k}{q^2} Q(\mathbf{q}) \exp(i\mathbf{q}\mathbf{r}) \frac{d^3 q}{(2\pi)^3} \quad (60)$$

where  $\varepsilon_{ik}^{(0)}(\mathbf{r})$  is the strain of the "undressed" crack and

$$Q(\mathbf{q}) = 2\pi \delta(q_z) \int \eta^2(x, y) \exp[i(q_1 x + q_2 y)] dx dy$$

is the Fourier-image of  $\eta^2(\mathbf{r})$ . The result (60) leads one to the following expression for the trace of the strain field:

$$\varepsilon_{ii}(\mathbf{r}) = \varepsilon_{ii}^{(0)}(\mathbf{r}) + \frac{A(1 - 2\sigma)}{2\mu(1 - \sigma)} \eta^2(\mathbf{r}) \quad (61)$$

The first term in the right-hand sides of any of the expressions (59), (60) and (61) describes the strain field generated by the "undressed" crack, while the second one yields the LPT contribution. Substitution of the strain trace (60, 61) into the free energy (5, 6, 7, 8) yields the effective free energy (17) with the factor  $\beta$  (16) in front of  $\eta^4$  instead of  $\beta_0$ .

## 7 Appendix B: Branching equation in the low-temperature phase

In the low-temperature phase the branching equation is mostly convenient to obtain starting from the effective free energy. The latter has the form:

$$F_{\text{eff}} = F_0 + I_2 (\alpha_{*2} - \alpha) \xi_2^2 + \frac{1}{3} I_3 \xi_2^3 + \frac{I_4 \beta}{4} \xi_2^4 \quad (62)$$

It differs from the expression (43) by the existence of the cubic term,  $I_3\xi^3$ , where

$$I_3 = \frac{1}{\sqrt{g\beta}} \int \Psi_*^3(r) \left( -\alpha\beta - \frac{\beta B \cos(\theta/2)}{\sqrt{r}} \right)^{1/2} r dr d\theta \quad (63)$$

Passing to dimensionless variables:  $r = \rho/R_2$ ,  $V = \nu V_c$  one finds:

$$I_3(\nu_2) = \int A(\rho, \theta) B(\rho, \theta) \rho d\rho d\theta \quad (64)$$

where

$$A(\rho, \theta) = \exp \left\{ 3 \times 2^{2/3} \sqrt{\rho} \cos(\theta/2) - 3 \times 2^{2/3} \rho [1 + \nu \cos(\theta)] \right\}$$

$$B(\rho, \theta) = \frac{3}{2 \times 2^{1/6}} \left[ (1 - \nu_2^2) \sqrt{\rho} - 2 \times 2^{1/3} \cos(\theta/2) \right]^{1/2}$$

The integrals  $I_2$  and  $I_4$  are defined as in (42).

The integrand of  $I_3$  becomes complex as soon as the expression  $(1 - \nu_2^2) \sqrt{\rho} - 2 \times 2^{1/3} \cos(\theta/2)$  under the radical becomes negative. This takes place along the line

$$\rho_0(\theta) = \frac{4 \times 2^{2/3} \cos^2(\theta/2)}{(1 - \nu_2^2)^2} \quad (65)$$

where  $\eta_0(\mathbf{r})$  (47) turns into zero. At smaller values of  $r$  one finds  $\eta = 0$ . For this reason in  $I_{1,2,3}$  one should only integrate over  $\rho$  from  $\rho_0(\theta)$  to infinity, while the integration over  $\theta$  runs from  $-\pi$  to  $\pi$ .

The integration has been done numerically using a standard NIntegrate routine of Mathematica 10.1 [70] employing an even-odd subdivision method with the local adaptive strategy. Below only the ratios  $I_2 I_4 / I_3^2$  and  $I_3 / I_4$  are used. These ratios and their fitting by simple functions:

$$s_1(\nu) = I_2 I_4 / I_3^2 \approx 0.59 + 3.13\nu_2 - 9.50\nu_2^2 + 9.00\nu_2^3 - 3.23\nu_2^4 \quad (66)$$

$$s_2(\nu) = I_3 / I_4 \approx 1.45 - 1.85\nu_2 + 2.44\nu_2^2 + \frac{0.31}{1 - 0.98\nu_2^2} \quad (67)$$

The effective free energy (62) has a cubic term. Since it is positive, one finds that the left minimum of the free energy (62) is more pronounced. Analogously to the static state one concludes that the solution of the branching equation should be chosen that corresponds to this deeper minimum, that is, the negative one. Let us note that in a general case the sign of  $\delta\eta$  is opposite to the one of  $\eta_0$ . Should we have chosen a negative  $\eta_0$ , we will get the positive sign for  $\delta\eta$ .

This solution of the branching equation takes the form:

$$\xi_2 = -\frac{s_2(\nu_2) B^{2/3}}{g^{1/6} \beta^{1/2}} \left\{ 1 + \sqrt{1 + s_1(\nu_2) \left[ 1 + 2 \frac{g^{1/3}}{B^{4/3}} \left( \alpha - \frac{\kappa^2 V^2}{8g} \right) \right]} \right\} \quad (68)$$

## 8 Appendix C. Simulation: technical details

To perform simulations we used the software COMSOL 4b. Equations have been simulated in a half-plane  $y \geq 0$ . A semi-circular domain has been defined with the diameter,  $D = 50$ . By trial and error we find that it is large enough, to let the solution vanish well far from the domain boundary. The initial mesh size of 5 has been chosen, but the adaptive mesh refinement option has been further used to automatically refine the mesh as appropriate. The no-flux boundary condition has been set at the boundary  $y = 0$  and the condition  $u = 0$

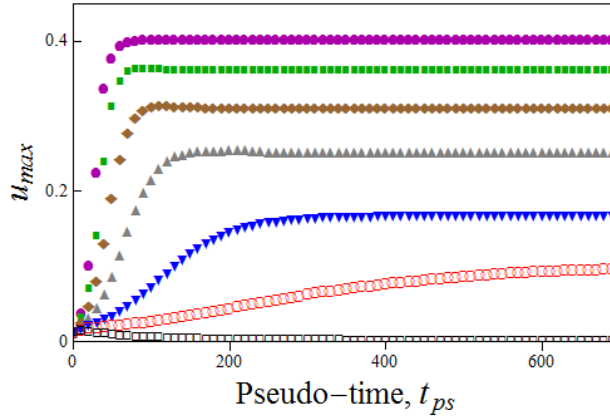


Figure 12: Illustration of the converging of the calculations with the pseudo-time showing the convergence of the amplitudes of the rescaled order parameter,  $u_{\max}$ , at different  $q$  values. Filled disks:  $q = 0.3$ , filled squares: 0.32, filled diamonds: 0.34, vertex-up triangles: 0.36, vertex-down triangles: 0.38, open circles: 0.39, empty squares: 0.41. Note that in the case of  $q = 0.39$  (point-down triangles) the  $u_{\max}(t)$  dependence still exhibits a slope and a for the satisfactory convergence a longer process was used (not shown).

at the rest of its boundary. A straightforward simulation of the static equation (53) with such boundary conditions, however, only returns the trivial solution  $u = 0$  at any value of the control parameter  $q$ . To avoid this instead of (53) we introduced a pseudo-dynamic equation:

$$\frac{\partial u}{\partial t_{\text{ps}}} = \Delta_1 u + 2^{1/3} \nu \frac{\partial u}{\partial x_1} - \left[ q - \frac{\left[ (x_1^2 + y_1^2)^{1/2} + x_1 \right]^{1/2}}{(x_1^2 + y_1^2 + \varepsilon)^{1/2}} \right] u - u^3 \quad (69)$$

where  $u = u(x_1, y_1, t_{\text{ps}})$ ,  $t_{\text{ps}}$  is the pseudo-time and  $\left[ (x_1^2 + y_1^2)^{1/2} + x_1 \right]^{1/2} / (x_1^2 + y_1^2 + \varepsilon)^{1/2}$  is equal to  $\cos(\theta/2)/r_1^{1/2}$ , regularized in the vicinity of the point  $r_1 = 0$  by a small parameter  $\varepsilon = 0.0001$ . Stable solutions of the static equation (53) represent fixed points of the dynamic system (69). As initial condition we used a smoothed step function, only unequal to zero in a vicinity of the point  $(0, 0)$ .

The dynamic system has been solved using the direct MUMPS solver with the BDF time stepping. The convergence of the solution to its fixed point has been controlled by the behavior of the  $u_{\max}$ , the maximum value of the function  $u(x_1, y_1, t_{\text{ps}})$ . By trials we found that 700 pseudo-time steps ensure a good convergence, though sometimes it has been necessary to keep the process as long as 3000 steps. Figure 12 shows the example of such a convergence study for a number of simulations in which all parameters except  $q$  were fixed, while  $q$  varied.

One can see that far from the bifurcation point the convergence takes place well before 700 pseudo-time steps are done. As it can be expected, the situation is different in the close vicinity of the bifurcation ( $q = 0.38$  and  $0.39$  corresponding to the vertex-down triangles and open circles in Fig. 12). Even here 700 pseudo-time steps guarantee a rather reliable convergence.

## References

- [1] S.J. Pennycook, Ultramicroscopy **123**, 28 (2012).

- [2] S. J. Wang et al., Nature Communications **67**, 45 (2014).
- [3] F. Meschke et al., J. Amer. Ceram. Soc. **83**, 353 (2000).
- [4] X. Tan et al., Acta Mater. **62**, 114 (2014)
- [5] S.D. Antolovich and D. Fahr, Eng. Fracture Mech. **4**, 133 (1972); E. Hornbogen, Acta Metall. **26**, 147 (1978).
- [6] S. K. Hann and J. D. Gates, J. Mater. Sci. **32**, 1249 (1997).
- [7] E. C. Oliver, et al., Appl. Phys. **A74**, S1143 (2002); Z. Khan and M. Ahmed, J. Mater. Eng. Perform. **5**, 201 (1996); M. K. Banerjee, N. R. Bandyopadhyay, and J. Mazumder, in *Processing and Fabrication of Advanced Materials Vi*, V. 1 & 2, (1998).
- [8] I. Roth et al., in *Esomat 2009 - 8th European Symposium on Martensitic Transformations*, (Eds. P. Sittner, P., V. Paidar and H. Seiner, 2009).
- [9] A. L. McKelvey and R. O. Ritchie, Metal. Mater. Trans. **A32**, 731 (2001); H. F. Lopez, Mater. Lett. **51**, 144 (2001); K. Kimura, T. Asaoka, and K. Funami, in Proc. Int. Conf. on Thermomech. Proc. of Steels and Other Materials, V. I-II, 1675 (1997); S. Gollerthan, et al., Acta Mater **57**, 5892 (2009); X. Wang and Z. Yue, in *Fracture and Damage Mechanics V*, Pts 1 and 2, Ed. by M. H. Aliabadi, Q. Li, L. Li and F. G. Buchholz, 2006), Vol. 324-325, p. 919.
- [10] S. W. Robertson et al., Acta Mater. **55**, 6197 (2007).
- [11] S. Daly et al., Acta Mater. **55**, 6322 (2007).
- [12] G. M. Loughran, T. W. Shield, and P. H. Leo, Int. J. Solids Struct. **40**, 271 (2003);
- [13] Y. H. Lu, et al., Intermetallics **10**, 823 (2002).
- [14] H. Qiu et al., Mater. Sci. Eng. **A579**, 71 (2013).
- [15] U.D. Hangen and G. Sauthoff, Intermetallics **7**, 501 (1999).
- [16] A. Paradkar et al., Metall. Mater. Trans. **40A**, 1604 (2009).
- [17] S. J. Wang et al., Nature Comm. **67** 45 (2014).
- [18] S.D. Antolovich, Trans. Met. Soc. AIME **242**, 2371 (1968).
- [19] I. Birkby and R. Stevens, Key Eng. Mater. **122-124**, 527 (1996);
- [20] P. M. Kelly and L. R. F Rose, Progr. Mater. Sci. **47**, 463 (2002).
- [21] R. I. Todd and M. P. S. Saran, Transformation toughening, in *Materials Processing Handbook* (Ed. J. R. Groza, Boca Raton, Fla., USA, CRC Press LLC, 2007), V. 20, 1-20.
- [22] S. O. Kramarov, N. Y. Egorov and L.M. Katsnel'son, Sov. Phys. - Solid State **28**, 1602 (1986); A. A. Grekov, Y. V. Dashko, S. O. Kramarov, et al., Ferroelectrics Lett. **8**, 59 (1988); C. S. Lynch, R. M. McMeeking, and Z. Suo, in *Second International Conference on Intelligent Materials. ICIM '94* edited by C. A. Rogers and G. G. Wallace (Technomic Publishing Co, Lancaster, PA, USA, 1994), p. 856.

- [23] G. G. Siu and W. G. Zeng, *J. Mater. Sci.* **28**, 5875 (1993).
- [24] T. Sasaki, et al., *J. Ceram. Soc. Japan* **120**, 473 (2012).
- [25] J. Karger-Kocsis and J. Varga., *J. Appl. Pol. Sci.* **62**, 291 (1996); J. Karger-Kocsis, J. Varga, and G. W. Ehrenstein, *J. Appl. Pol. Sci.* **64**, 2057 (1997); H.-J. Sue, J. D. Earls, and R. E. Hefner, Jr., *J. Mater. Sci.* **32**, 4039 (1997); T. K. Sung et al., *J. Mater. Sci.* **33**, 2421 (1998); S. T. Kim et al., *J. Mater. Sci.* **33**, 2421 (1998); G. A. Maier et al., *Macromolecules* **38**, 6099 (2005); T. Koyama, T. Araki, and H. Tanaka, *Phys. Rev. Lett.* **102**, 065701 (2009).
- [26] J. A. Donovan, *Nippon Gomu Kyokaishi* **75**, 239 (2002); S. Trabelsi, P.-A. Albouy, and J. Rault, *Macromolecules* **35**, 10054 (2002); H. P. Zhang et al., *Phys. Rev. Lett.* **102**, 245503 (2009). J.-B. Le Cam and E. Toussaint, *Macromolecules* **43**, 4708 (2010); N. Saintier, G. Cailletaud, and R. Piques, *Mater. Sci. Eng.* **A528**, 1078 (2011).
- [27] K. Nishimura and N. Miyazaki, *Cmes-Comp. Model. Eng. Sci.* **2**, 143 (2001);
- [28] Y.-F. Guo and D.-L. Zhao, *Mater. Sci. Eng.* **A448**, 281 (2007); Y.-F. Guo, Y.-S. Wang, and D.-L. Zhao, *Acta Mater.* **55**, 401 (2007).
- [29] A. Latapie and D. Farkas, *Modell. Simul. Mater. Sci. Eng.* **11**, 745 (2003); R. Matsumoto et al., *Cmes-Comp. Model. Eng. Sci.* **9**, 75 (2005); I. R. Vatne et al., *Mater. Sci. Eng.* **A560**, 306 (2013).
- [30] M. J. Buehler et al., *Phys. Rev. Lett.* **99**, 165502 (2007).
- [31] D. Sherman, M. Markovitz and O. Barkai, *J. Mech. Phys. Solids* **56**, 376 (2008); F. Atrash and D. Sherman, *J. Mech. Phys. Solids* **60**, 844 (2012).
- [32] J. R. Kermode et al. *Nature* 455,1224 (2008);
- [33] J. Mei, et. al., *Int. J. Solids Struct.*, **48**, 3054 (2011).
- [34] M. Ruda, D. Farkas, and G. Bertolino, *Comp. Mater. Sci.* **49**, 743 (2010).
- [35] Y. Zhang et. al., *J. Nucl. Mater.* **430**, 96 (2012).
- [36] A. Falvo et al., *J. Mater. Eng. Perform.* **18**, 679 (2009).
- [37] A. Boulbitch and A. L. Korzhenevskii, *Phys. Rev. Lett.* **107**, 085505 (2011).
- [38] L. B. Freund, *Dynamic Fracture Mechanics*. (Cambridge University Press, Cambridge, 1998).
- [39] G. P. Cherepanov, *Mechanics of brittle fracture*. (McGraw Hill, New York, London, 1979).
- [40] J. Fineberg and M. Marder, *Phys. Rep.* **313**, 1 (1999).
- [41] J. E. Field, *Cont. Phys.* **12**, 1 (1971).
- [42] H. Gao, *J. Mech. Phys. Solids* **44**, 1453 (1996); M. J. Buehler and H. Gao, *Nature* **439**, 307 (2006).
- [43] E. Bouchbinder, A. Livne and J. Fineberg, *Phys. Rev. Lett.* **101**, 264302 (2008).

- [44] J. A. Hauch et al., Phys. Rev. Lett. **82**, 3823 (1999).
- [45] A. Bertram and J.F. Kalthoff, Key Eng. Mater. **251-252**, 423 (2003).
- [46] B. L. Karihaloo and J. H. Andreasen, *Mechanics of Transformation Toughening and Related Topics* (Elsevier Science Ltd Amsterdam, The Netherlands, 1996).
- [47] V.M. Nabutovskii and B.Ya. Shapiro, Sov. Phys. JETP **48**, 480 (1978).
- [48] A.L. Korzhenevskii, Sov. Phys. Solid State **28**, 745 (1986); *idem*, *ibid* **28**, 1999 (1986).
- [49] A. Boulbitch and P.E. Pumpyan, Sov. Phys. Crystallogr. **35**, 156 (1990).
- [50] A. Boulbitch and Yu. M. Gufan, Sov. Phys. JETP **67**, 1153 (1988); *idem*, Ferroelectrics **98**, 277 (1989).
- [51] A. Boulbitch and P.E. Pumpyan, Ferroelectrics **124**, 11 (1991); *idem*, *ibid* **111**, 111 (1990); *idem* J. Phys.I **3**, 1175 (1993); A. Boulbitch, V.P. Dmitriev, O.A. Zhelnova and P.E. Pumpyan, Sov. Phys. JETP **71**, 619 (1990)
- [52] A. A. Boulbitch, J. Mater. Sci. **27**, 1070 (1992).
- [53] A. Boulbitch and P. Toledano, Phys. Rev. Lett. **81**, 838 (1998).
- [54] V. I. Levitas, Int. J. Plasticity **16**, 805 (2000); *idem*, *ibid*, **16**, 851 (2000); A. V. Idesman, V. I. Levitas, E. Stein, *ibid*, **16**, 893 (2000).
- [55] C. Bjerken and A. R. Massih, ArXiv: Condensed Matter 1110.1292v (2011).
- [56] T. Koyama, T. Araki, and H. Tanaka, Phys. Rev. Lett. **102**, 065701 (2009); H. Bai, Y. et. al., J. Polymer Sci. **B47**, 46 (2009); G. M. Wallner et al., Polymer Testing **27**, 392 (2008); G. A. Maier et al., Macromolecules **38**, 6099 (2005).
- [57] P. C. Hohenberg and B. I. Halperin, Rev. Mod. Phys. **49**, 435 (1977)
- [58] L. D. Landau and E. M. Lifshitz, *Statistical Physics*. (Pergamon Press, Oxford, 1985).
- [59] Yu. M. Gufan, *Structural Phase Transitions*, (Moscow, Nauka, 1983) - in Russian
- [60] J. C. Toledano and P. Toledano, *The Landau Theory of Phase Transitions*. (World Scientific, Singapore, 1987).
- [61] The same condition is valid for any other order parameter.
- [62] V. G. Vaks, *Introduction into Microscopic Theory of Ferroelectrics* (Nauka, Moscow, 1973) - in Russian
- [63] L. D. Landau, E. M. Lifshitz, and L. P. Pitaevskii, *Statistical Physics. Theory of the Condensed State*. (Butterworth Heinemann, Oxford, 2002).
- [64] L. D. Landau and E. M. Lifshitz, *Electrodynamics of Continuous Media* (Elsevier Butterworth-Heinemann, Oxford, 2004).
- [65] It only accounts for the dissipation due to the evolution of the order parameter, rather than acoustic degrees of freedom. To account for the dissipation of the latter one needs to add the corresponding terms to the dissipation function. This is, however, not done in the present paper.

- [66] L. D. Landau and E. M. Lifshitz, *Theory of Elasticity* (Pergamon Press, Oxford, 1986).
- [67] V. I. Smirnov, *A Course in higher mathematics. Integral equations and partial differential equations.* (Pergamon Press, Oxford, London, Edinburgh 1964).
- [68] M. M. Vainberg and V. A. Trenogin, *Theory of branching of solutions of non-linear equations* (Noordhoff, Leyden, 1974).
- [69] G. Legrain, N. Moes and T. Belytschko, Int. J. Numer. Meth. Engng, 46, 131 (1999); G. Legrain, N. Moes and E. Verron. *idem* **63**, 290 (2005).
- [70] Wolfram Research, Inc., Mathematica, Version 10.0, Champaign, IL (2014).
- [71] L.-Q. Chen, Topics in Appl. Phys. **105**, 363 (2007).
- [72] D.A. Scrymgeour, V. Gopalan, A. Itagi, A. Saxena and P.J. Swart, Phys. Rev. **B71**, 184110 (2005).
- [73] S. Panteny, C.R. Bowen and R. Stevens, J. Mater. Sci. **41**, 3837 (2006); B. Ertug et al., Acta Phys. Pol. **A123**, 188 (2012); R.F. Cook, C.J. Fairbanks, B.R. Lawn and Y.W. May, J. Mater. Res. **2**, 345 (1987).
- [74] S. G. Jabarov et al. Phys. Solid State **53**, 2300 (2011).
- [75] T. Ishidate et al., Phys. Rev. Lett. **78**, 2397-2400 (1997).
- [76] I. Tomeno and S. Matsumura, J. Phys. Soc. Jap. **56**, 163 (1987).
- [77] H. Igawa, T. Mori and S. Kojima, Jap. J. Appl. Phys. **53**, 05FE01 (2014).
- [78] A. He, H. Huang, and L. Zhou, in *Advances in Abrasive Technology XV*, edited by Y. F. Zhang, et al., (2012), Vol. 565, p. 564.
- [79] J. Shi, Q. Zhang and G. Yang, Wuji Cailiao Xuebao **4**, 8 (1989).
- [80] H. Vogt, J.A. Sanjurjo and G. Rossbroich, Phys. Rev. **B26**, 5904 (1982); I. Ponomareva, L. Bellaiche, T. Ostapchuk et al. Phys. Rev. **B77**, 012102 (2008); F. Wan, J.G. Han and Z.Y. Zhu, Phys. Lett. **A372**, 2137 (2008).
- [81] J. Hlinka, B. Hehlen, A. Kania et al., Phys. Rev. **B87**, 064101 (2013).
- [82] H. Lehnert et. al. Z. Kristallographie **212**, 712 (1997).
- [83] [https://en.wikipedia.org/wiki/Barium\\_titanate](https://en.wikipedia.org/wiki/Barium_titanate)
- [84] <http://www.thermograde.com/lead-titanate-pbti03->
- [85] <http://www.roditi.com/SingleCrystal/LiNbO3/liNBO3-Properties.html>
- [86] R. Blinz and B. Zeks, *Modes in Ferroelectrics and Antiferroelectrics.* (North-Holland Publishing Company, New York, 1974).
- [87] M. A. Krivoglaz, *Theory of X-ray and thermal – neutron scattering by real crystals.* (Plenum Press, New-York, 1969).
- [88] E. Y. Tonkov, *High Pressure Phase Transformations: A Handbook: v. 1-3* (Gordon and Breach SA, Amsterdam, 1992).

- [89] J. Jones and M. Hoffman, J. Am. Ceram. Soc. **89**, 3721 (2006).
- [90] See tables pp. 889-902 in the book [39]
- [91] A. Karma, D.A. Kessler and H. Levine, Phys. Rev. Lett. **87**, 045501 (2001); V. Hakim and A. Karma, Phys. Rev. Lett. **95**, 235501 (2005); R. Spatschek, M. Hartmann, E. Brener and H. Mueller-Krumhaar, Phys. Rev. Lett. **95**, 2015502 (2006).
- [92] M.C. Cross, and P.C. Hohenberg, Rev. Mod. Phys. **65**, 851 (1993).
- [93] F. Rostom, A. Royne, D.K. Dysthe and F. Renard, Tectonophysics **583**, 68 (2013).
- [94] A. Boulbitch and A.V. Fisenko, Phys. Lett. **A243**, 5 (1998).